Research Square

Preprints are preliminary reports that have not undergone peer review.
They should not be considered conclusive, used to inform clinical practice,
or referenced by the media as validated information.

A Lifespan Normative Reference for Spectral Signatures of Brain Activity

Francesco Mallus

francesco.mallus@outlook.com

University Hospital Tübingen, Tübingen, Germany

Yanwu Yang

Tuebingen University Hospital; Max-Planck Institute for Intelligent Systems, Tübingen, Germany; German Center for Mental Health (DZPG), partner site Tübingen, Germany https://orcid.org/0000-0002-7547-4580

Seyed Mostafa Kia

Tilburg University https://orcid.org/0000-0002-7128-814X

Tijl Grootswagers

Western Sydney University https://orcid.org/0000-0002-7961-5002

Abraham Nunes

Dalhousie University

Tomas Ros

University of Geneva

Thomas Wolfers

Department of Psychiatry and Psychotherapy, University Hospital Tübingen https://orcid.org/0000-0002-7693-0621

Article

Keywords: Normative modeling, Electroencephalography (EEG), spectral features, lifespan, neurodegeneration, neurocognitive and neurodevelopmental disorders

Posted Date: May 5th, 2026

DOI: https://doi.org/10.21203/rs.3.rs-9544150/v1

License: This work is licensed under a Creative Commons Attribution 4.0 International License.
Read Full License

Additional Declarations: There is **NO** Competing Interest.

A Lifespan Normative Reference for Spectral Signatures of Brain Activity

Francesco Antonio Mallus[1,2], Yanwu Yang[1,3,4], Seyed Mostafa Kia[5], Tijl Grootswagers[6], Abraham Nunes[7], Tomas Ros[8], Thomas Wolfers [1,9,10]*

1 Department of Psychiatry and Psychotherapy, University Hospital Tübingen, Tübingen, Germany

2 Graduate Training Center of Neuroscience, International Max-Planck Research School, Tübingen, Germany

3 Max-Planck Institute for Intelligent Systems, Tübingen, Germany

4 German Center for Mental Health (DZPG), partner site Tübingen, Germany

5 Center of Cognitive Science and Artificial Intelligence, Tilburg University, Tilburg, the Netherlands.

6 The MARCS Institute for Brain, Behaviour and Development, Western Sydney University, Sydney, Australia

7 Department of Psychiatry, Dalhousie University, Halifax, Nova Scotia

8 CIBM Center for Biomedical Imaging, University of Geneva, Geneva, Switzerland

9 German Center for Mental Health (DZPG), Jena-Magdeburg-Halle, Jena, Germany

10 Department of Clinical Psychology, Friedrich Schiller University Jena, Jena, Germany

* Corresponding Authors:

Francesco Mallus

Laboratory for Mental Health Mapping (MHM-Lab)

Department of Psychiatry and Psychotherapy

University Hospital Tübingen, Tübingen, Germany

francesco.mallus@outlook.com

Prof. Dr. Thomas Wolfers

Carl-Zeiss Professor for AI in Neural Systems Imaging

Laboratory for Mental Health Mapping (MHM-Lab)

Friedrich Schiller University Jena, Jena, Germany

dr.thomas.wolfers@gmail.com

Keywords: Normative modeling; Electroencephalography (EEG); spectral features; lifespan; neurodegeneration; neurocognitive and neurodevelopmental disorders

Abstract: Spectral features derived from electroencephalography (EEG) have long been proposed as biomarkers of brain dysfunction, yet few have gained consensus or entered clinical practice. A key obstacle is the lack of harmonized, lifespan-covering EEG resources, which has limited the development of generalizable models and stalled progress towards cost-effective individualized markers of brain health. Here we chart lifespan trajectories of spectral EEG features based on 3,973 individuals (5,600 recordings, ages 1–82, ten sites, >200 hours of resting-state EEG). Using distributional regression, we fit 231 models across 21 spectral features and 11 cortical regions, jointly adjusting for age, sex, recording paradigm, data quality, and acquisition site. Critically, these models capture not only how spectral features shift across the lifespan but how their variability evolves and generalize robustly out-of-sample (n = 400; median z-score mean = 0.019, SD = 1.047). Across six diagnostic groups, neurocognitive disorders yielded the strongest deviation signatures (Alzheimer's disease AUC = 0.95; frontotemporal dementia AUC = 0.91), and we provide the first normative-referenced characterization of aperiodic spectral features in neurodegeneration. Neurodevelopmental and mental health conditions showed marked heterogeneity and in the largest normative evaluation of the theta-to-beta ratio in ADHD to date (n = 1,034), this established biomarker failed to replicate. Together, these findings consolidate decades of lifespan EEG research into a transferable normative reference, laying the foundation for individualized assessment of brain function and enabling scalable, low-cost tools for early detection and treatment monitoring.

Introduction

Resting-state electroencephalography (EEG) is a central tool in neurology and psychiatry and one of the most versatile techniques in systems neuroscience [1,2]. Routine visual inspection of EEG signals supports diagnosis and monitoring in epilepsy, encephalopathy, dementia, and a range of neuropsychiatric conditions [1,3], while quantitative EEG extracts spectral and topographic features that have been proposed as potential biomarkers of brain dysfunction [2,4]. Canonical spectral measures capture complementary aspects of spontaneous cortical dynamics during eyes-open and eyes-closed rest [4,5], and several of these features have been associated with neuropsychiatric conditions [6,7]. However, due to the intrinsic complexity and heterogeneity of brain disorders, only a limited number of electrophysiological findings have reached broad consensus and even fewer have translated into clinically approved applications [2]. Despite decades of database initiatives [8,9], fully harmonized lifespan EEG resources remain scarce compared to neuroimaging modalities [10,11], limiting the development of robust, generalizable models and constraining progress toward individualized, cost-effective markers of brain health.

Akin to growth charts in pediatric medicine, where a child's height or weight is interpreted relative to age- and sex-appropriate population centiles rather than a binary normal/abnormal threshold, normative modelling estimates the full conditional distribution of brain measures as a function of age, sex, site, and recording paradigm in a reference population, expressing each individual's observation as a standardized deviation score [12]. Rather than asking whether a diagnostic group differs from controls on average, this framework asks how far and in which direction each person departs from expectation given their demographic and acquisition context. Stacking these deviations across spectral features and cortical regions embeds each individual in a multivariate electrophysiological distance space, enabling principled, comparable quantification of abnormality at the individual rather than the group level [10,12–16]. This approach is particularly well suited to the heterogeneity and diagnostic overlap that characterize neuropsychiatric conditions in EEG and beyond [13,16,15,17]. The conditions examined here span neurocognitive disorders such as Alzheimer's disease and frontotemporal dementia [7,18,19], neurodevelopmental conditions including ADHD [20] and ASD [21,22] as well as anxiety disorders [23] and PTSD [21,24], which frequently share overlapping symptoms, trajectories, and exhibit substantial within-

group variability [22,25]. Traditional case-control designs cannot resolve this heterogeneity or generalize findings to individuals, while a normative framework situates each person within a population reference, revealing distinct electrophysiological phenotypes even where diagnostic labels overlap.

Here we establish a lifespan normative reference for resting-state spectral EEG, modelling narrow-band relative powers, band ratios, aperiodic 1/f slope and intercept [5], and peak alpha frequency across eleven cortical regions [26] in 3,973 individuals (ages 1-82, ten sites). Using GAMLSS (Generalized Additive Models for Location, Scale and Shape) [5,25,27], 231 models were jointly adjusted for age, sex, recording paradigm, site, and data quality, capturing not only how spectral features shift across the lifespan but how their variability evolves, a dimension inaccessible to conventional approaches. From these models we derive centile trajectories and individual z-scores, and apply them to six neuropsychiatric conditions, revealing a clear hierarchy of spectral abnormality. Neurocognitive disorders produce the strongest signatures. In Alzheimer's disease, the theta-to-alpha ratio yields the largest effect observed across all conditions ($r = +0.79$), and we report the first normative-referenced characterization of aperiodic dynamics in both Alzheimer's disease and frontotemporal dementia. Neurodevelopmental conditions show smaller, heterogeneous deviations and in the largest normative evaluation of the theta-to-beta ratio in ADHD to date ($n = 1,034$), this FDA-cleared biomarker could not be replicated. Anxiety spectrum disorders display a novel aperiodic elevation consistent with broadband arousal dysregulation, while PTSD shows no significant group-level deviation. Together, these results unify decades of fragmented EEG lifespan research into a single normative reference, reveal novel spectral signatures of impaired brain health, and establish a principled foundation for individualized characterization of brain function across the lifespan.

[Insert Figure 1]

Results

We split the non-diagnosed cohort into a training set ($n = 1,427$; 1,890 recordings) and an independent held-out reference set ($n = 400$; 678 recordings) used for all clinical comparisons. The 21 spectral features comprised narrow-band relative powers (δ, θ, α, β, γ; fractional and decibel), peak alpha frequency, three ratios (θ/β, θ/α, fast/slow), and aperiodic slope and intercept (see Methods). Six

diagnostic groups were projected into this space: Alzheimer's disease (n = 36), FTD (n = 22), ADHD (n = 1,034), ASD (n = 174), anxiety disorders (n = 272), and PTSD (n = 35). We report model validation, lifespan trajectories, univariate and multivariate deviation profiles, and robustness to sex, recording condition, and age (Figure 1; Supplementary Tables S1–S2).

Robust out-of-sample generalization and well calibrated normative deviation scores

As mentioned above, model performance was evaluated out-of-sample in a held-out, non-diagnosed reference cohort (n = 400) matched to the training sample on age, sex, and site, while the model specifications were finalized on training data only. All metrics were computed on quantile residuals, z-scores from the probability integral transform, which under correct specification follow N (0,1) regardless of the original feature scale, making summary statistics directly comparable across all 231 models. Predictive performance generalized well with median held-out RMSE = 0.61 (IQR = 0.72; median absolute train–test gap = 0.08), MSE = 0.37 (IQR = 0.82; gap = 0.32), and R^2 = 0.31 (IQR = 0.28), modestly below training (R^2 = 0.37, IQR = 0.19; gap = 0.09). Point-prediction accuracy, however, is not the primary requirement for normative modelling, the key criterion is well-calibrated distributional fits. On this criterion, the held-out cohort performed well. Z-score distributions closely matched the expected N (0,1) standardization, with median mean = 0.019 (IQR = 0.005) and SD = 1.047 (IQR = 0.002); ~90% of models had $|\mu| \leq 0.1$ and 100% had σ within [0.8, 1.2]. Skewness (0.036, IQR = 0.24) and excess kurtosis (0.40, IQR = 0.54) were near zero, and residuals were highly normal (median Filliben statistic = 0.995, IQR = 0.001; Supplementary Table S3). Adding independent component analysis (ICA) to the preprocessing pipeline produced no meaningful change in model quality and z-score residual and prediction metrics were statistically indistinguishable after multiple-comparison correction (all $q > 0.8$). Only ΔR^2 reached significance ($\mu = 0.084$, $q = 8 \times 10^{-4}$, effect size 0.54), yet lifespan trajectories, quantile spreads, and covariate effects remained highly consistent (Supplementary Table S4). Together, these results demonstrate well-calibrated normative deviation scores that generalize out-of-sample and are robust to preprocessing choices.

Lifespan trajectories of spectral brain signatures

[Insert Figure 2]

Across lobar regions and both sexes, narrow-band trajectories showed a uniform normative redistribution from slow to fast activity, with the largest absolute slopes before ~20 years across all features (Figure 2). For each feature, we summarize median (50th centile) and dispersion (3rd-97th centile) trends averaged across lobes, with turning points where present (Supplementary Table S5b). Slow bands declined consistently across the lifespan. Delta decreased steeply during childhood and adolescence (median slope -10.0×10^{-3} Fractional Band Power (FBP)/year) before decelerating, yielding a net median change of -0.25 FBP and dispersion rose until ~30 years and stabilized. Theta declined more modestly (-1.0×10^{-3} FBP/year) but reversed direction in middle age, so this late-life rise left a net change of only -0.02 FBP with near-constant variance. Fast bands showed the complementary pattern. Beta rose rapidly in early life (4.0×10^{-3} FBP/year until 20 years; net change +0.17 FBP), with dispersion following a similar rise-and-stabilize profile. Gamma rose more slowly but monotonically (0.8×10^{-3} FBP/year; net change +0.05 FBP), with parallel increases in dispersion. Alpha followed an inverted-U trajectory, rising fast in childhood (+4.1×10^{-3} FBP/year from 1-20 years) and decreasing after ~25 (-1.1×10^{-3} FBP/year) for a near-zero net change (-0.009 FBP) and dispersion also rose, peaking around 20 years before declining. Peak alpha frequency (PAF) mirrored alpha power but diverged at older ages. After the early-adulthood peak, PAF moved toward a local minimum near ~44 years, followed by late-life stabilization. The slow-to-fast redistribution was accentuated in the dB representation with delta and theta dropping over the lifespan (net −2.19 dB, −0.67 dB), while beta and gamma rose fast and strongly (+7.87 dB, +5.58 dB). The steepest slopes again occurred before ~25 years (beta = 0.28 dB/year; gamma = 0.18 dB/year, ages 1–20), with positive slopes sustained through adulthood. Aperiodic components (1/f slope and intercept) diminished monotonically across the lifespan, mirroring overall spectral changes at each phase with faster declines at developmental ages, clear deceleration from early adulthood, and a subtle inflection in middle adulthood (~43 years for slope, ~59 for intercept). Band-ratio trajectories recapitulated the narrow-band interplay with theta/beta and alpha/beta decreased consistently, while fast/slow, gamma/beta, and theta/delta rose steadily.

Sex-specific normative trajectories were highly similar across all features and regions. None of the 143 shape comparisons showed evidence of sex differences after FDR correction (min q = 0.55, mean q = 0.98; Figure S8), and the same held for dispersion (min q = 0.58, mean q = 0.96). Small but significant level offsets appeared in 33/143 comparisons (23.1%; min q = 0.003, mean q = 0.59), but were feature- and region-specific rather than globally consistent across the scalp (Figure 2a). Any qualitative female-male offset visible in individual plots should therefore be interpreted cautiously and within uncertainty bands, as broad, spatially consistent sex effects were not supported. Left-right homolog comparisons provided no evidence for lateralization after correction (n = 64; 0% with q < 0.05). To quantify regional asymmetries, we compared intra-hemispheric region pairs using a permutation test on the absolute area difference between q50(age) trajectories (Figure S9). Across all 240 region-band-sex comparisons, the mean permutation p-value was 0.94 (Figure S10), and all FDR-corrected q-values equaled 1.0, no comparison reached significance, indicating no substantial sex or topographic differences in modeled spectral features across the lifespan (Supplementary S5).

All normative trends replicate prior results[5,9,28–33] depicting a coherent lifespan continuum with two hallmarks. A growth spurt to early adulthood (~1-20 years) with decelerating slow-band and aperiodic declines, decelerating fast-band rises, and peaks in alpha power and mid-adulthood inflection points (~43-59 years) where slow bands and alpha resume declining and PAF stabilizes.

Feature level spectral signatures across neuropsychiatric conditions

[Insert Figure 3]

Alzheimer's disease (n = 36, 49–79 years, 67% female). All features except gamma differed significantly from normative expectation (adjusted p-value (q) < 0.001), with medium-to-large effect sizes ($|r| \in [0.28, 0.79]$). The canonical spectral slowing pattern was clearly replicated with elevated delta (+0.44, q<0.001) and theta (+0.66, q<0.001) alongside reduced alpha (−0.65, q<0.001) and beta (−0.60, q<0.001), confirming established spectral signatures [3,18,34–36]. PAF was significantly slowed (−0.28, q<0.05). Band ratios amplified these patterns with theta-alpha ratio showing the largest effect in general (+0.79, q<0.001) [19], followed by fast-slow ratio (−0.68, q<0.001) [7,35] and theta-beta ratio

(+0.66, q<0.001) [37]. Gamma showed a mild, non-significant positive deviation. Beyond these confirmatory findings, the normative framework enabled, for the first time, age-referenced quantification of aperiodic components in Alzheimer's disease. The 1/f slope was steeper than normative expectation (+0.34, q<0.01), indicating a relative concentration of power at low frequencies, mechanistically distinct from, though consistent with, the narrow-band slowing above. The 1/f intercept showed one of the largest deviations in general (+0.58, q<0.001), reflecting elevated broadband power underlying the observed slow-frequency excess and potentially reflecting compromised synaptic integration and a breakdown in coordinated large-scale network function characteristic of neurocognitive decline.

Frontotemporal dementia (FTD: n = 22, 44–78 years, 41% female). Deviations followed the same direction as Alzheimer's disease but with attenuated effect sizes ($|r| \in [0.33, 0.72]$). Theta (+0.61, q<0.001) and alpha (−0.52, q<0.001) remained strongly significant, delta (+0.33, q<0.05) and beta (−0.37, q<0.01) showed reduced significance and gamma was non-significant. In contrast to Alzheimer's disease, PAF showed no significant deviation. Band ratios were strongly deviated and theta-beta (+0.51, q<0.001), theta-alpha (+0.72, q<0.001), and fast-slow (−0.59, q<0.001), all reinforcing the narrow-band pattern. Among aperiodic components, only the 1/f intercept reached significance (+0.42, q<0.01) and 1/f slope did not. To our knowledge, this constitutes the first normative-referenced characterization of aperiodic features in FTD.

Attention-Deficit/Hyperactivity Disorder (ADHD: n = 1,034, 5–22 years, 65% male). Intra-group variability was pronounced and effect sizes uniformly small ($|r| \in [0.12, 0.18]$). Theta power was significantly elevated (+0.14, q<0.001), confirming the most replicated spectral finding in ADHD [6,38,39]. Delta was suppressed (−0.15, q<0.001), extending prior literature in which slow-wave deviations are predominantly reported as a composite [25,38]. Alpha power was significantly above norm (+0.18, q<0.001), opposing the decreased alpha typically reported in case-control studies [38,39], though effect sizes in that literature have been modest and variable [25,38] and the present sample substantially exceeds those on which the original consensus was established. Beta, gamma, and PAF did not reach significance. The theta-beta ratio, previously proposed [40] and recently disputed [41] as a biomarker, was also non-significant. Theta-alpha (−0.12, q<0.01) and fast-slow (+0.15, q<0.001) ratios proved more

sensitive to the observed spectral redistribution. Among aperiodic features, 1/f intercept was significantly elevated (+0.12, q<0.01); 1/f slope was not.

Autism Spectrum Disorder (ASD: n = 174, 5–22 years, 62% male). The deviation profile was strikingly similar to ADHD. Theta showed the largest narrow-band effect (+0.21, q<0.001), extending meta-analytic literature in which the group effect of theta was near-zero [42]. Delta was again suppressed (−0.17, q<0.01). Alpha was significantly above norm (+0.15, q<0.01), in discordance with the consensus identifying reduced relative alpha as the most consistent spectral alteration in ASD [42], though substantial inter-study heterogeneity has been noted across all frequency bands [42,43]. Beta, PAF, and aperiodic components did not reach significance. Gamma was significantly elevated (+0.14, q<0.05), confirming a strong spectral finding in the ASD literature [42,44]. The fast-slow ratio was the only ratio to reach significance (+0.15, q<0.01), consistent with the narrow-band pattern. Direct comparison between ADHD and ASD revealed no significant feature-level difference (all q > 0.29) in both shared suppressed delta, elevated theta, and above-norm alpha with small effects and considerable within-group spread.

Anxiety Disorders (n = 272, 5–22 years, 60% female). The deviation pattern was sparse. Among narrow-band features, only alpha reached significance (+0.12, q<0.05) and delta, theta, beta, gamma, and PAF did not. The 1/f intercept showed a significant positive deviation (+0.15, q<0.01), while 1/f slope did not. To our knowledge, this is the first normative-referenced aperiodic characterization across the anxiety spectrum. The fast-slow ratio reached marginal significance (+0.11, q<0.05); theta-alpha and theta-beta ratios did not. *Post-Traumatic Stress Disorder (PTSD: n = 35, 5–21 years, 77% female).* No feature reached significance after FDR correction. Deviation directions were broadly consistent with the anxiety profile, below-norm delta, above-norm theta, elevated 1/f intercept, but effect sizes were too small to survive correction. PAF showed the largest absolute effect in this group (-0.21, q = 0.058). These results are consistent with the growing recognition that diagnostic boundaries do not map onto discrete spectral phenotypes [2,25,39,42,43] and that individual-level deviation profiles may be more informative than group-level contrasts for neurodevelopmental and mental health conditions [9,12,15,16,45].

Robust multivariate spectral signatures across neuropsychiatric conditions

To move beyond univariate comparisons, we pooled all 11 spectral features into a multivariate z-score space. In the theta-beta subspace, the pair with the strongest cross-diagnostic effects in the literature [6,41,46], 95% confidence ellipses separated Alzheimer's disease and FTD from the reference, while all other groups overlapped substantially (Figure 3c). The pattern held across alternative feature pairs and triplets. Mahalanobis distance D^2 across all 11 features confirmed this ordering (Supplementary S7) with Alzheimer's disease (9.18 ± 3.20) and FTD (7.41 ± 3.87) showed the largest displacement, whereas PTSD (3.17 ± 1.02), ASD (2.82 ± 0.93), anxiety disorders (2.77 ± 1.03), and ADHD (2.30 ± 0.73) clustered at markedly lower, largely indistinguishable distances.

Symmetric within-category D^2 indicated limited separability between clinically related conditions with Alzheimer's vs FTD (4.74), anxiety vs PTSD (3.59), and ADHD vs ASD (3.29) (Supplementary Table S7b). Binary LDA classifiers (10-fold group-aware CV, Figure 3d, Supplementary Table S10) reproduced this, with Alzheimer's (AUC = 0.95) and FTD (0.91) discriminated most accurately and ASD (0.61), ADHD (0.59), anxiety (0.57), and PTSD (0.55) at modest accuracy. Permutation testing (10,000 iterations) was significant for all conditions ($p < 0.001$) except anxiety disorders and PTSD, and within-category classifiers performed at or near chance (ADHD vs ASD AUC = 0.58, $p = 0.005$; Alzheimer's vs FTD 0.52; anxiety vs PTSD 0.53). Multiclass one-vs-rest classification yielded micro-average AUC = 0.85 and macro-average 0.64, with only anxiety ($p = 0.10$) and PTSD ($p = 0.55$) failing permutation significance (Supplementary Figure S1; Table S10).

[Insert Figure 4]

We next stratified individual D^2 by sex, recording condition, and age while acquisition site was not stratified, as instrumental variation is absorbed as a random effect during normative modeling (Supplementary Table S8). Sex comparisons against sex-stratified references yielded no significant effects in any cohort, indicating that sex-related spectral variance is fully captured by the normative model. Eyes-closed vs eyes-open differences were significant but very small, and only in ADHD (+0.06, $q < 0.05$) and anxiety disorders (+0.16, $q < 0.01$). while neurocognitive cohorts lacked eyes-open data. Age-binned trajectories (Figure 4d) showed stable, low-magnitude deviations across 4-22

years for neurodevelopmental and mental-health conditions and persistently elevated deviations across 56-80 years for Alzheimer's and FTD, with eyes-closed and eyes-open curves overlapping. Regional classification maps (Figure 4a) revealed no lobar effects surviving correction (Supplementary Table S9), consistent with spatially distributed rather than focal deviations.

Together, neurocognitive disorders produce classifiable broadband signatures spanning delta, beta, gamma, and their ratios, whereas neurodevelopmental and most mental-health conditions manifest as diffuse, low-magnitude deviations that no single feature reliably captures, the 1/f intercept in anxiety disorders being the notable exception. Because feature choice directly shapes multivariate distance, profiling requires the full feature set, which is robust to all tested confounds. These findings motivate a shift toward individual-level distance profiling, better suited to the overlapping, comorbidity-rich nature of mental and neurocognitive health conditions.

Discussion

We establish a large-scale lifespan normative reference for resting-state spectral EEG, 231 feature-region models that generalize robustly out of sample with well-calibrated deviation scores. Applied to six neuropsychiatric conditions, the framework reveals a clear hierarchy of spectral abnormality. Neurocognitive disorders produce the strongest and most consistent deviation profiles. In Alzheimer's disease, the theta/alpha ratio yields the largest effect size across all conditions and features (rank-biserial = +0.79), and we provide the first normative-referenced characterization of aperiodic EEG signatures in both Alzheimer's disease and frontotemporal dementia. In ADHD, the largest normative-referenced evaluation of the theta/beta ratio to date (n = 1,034) finds it non-significant, the strongest evidence yet against its standing as a standalone diagnostic biomarker. ADHD and ASD are spectrally indistinguishable at the group level, and anxiety spectrum disorders and PTSD produce sparse, unreliable deviation profiles. Together, these findings consolidate lifespan EEG research into a unified normative reference of unprecedented scale, surface novel spectral patterns of neurodevelopment and impaired brain health, and lay a quantitative foundation for individualized, multivariate characterization of brain function, with scalable, low-cost applications in early detection and treatment monitoring (Figure 5).

[Insert Figure 5]

Lifespan trajectories and individual-level inference

The normative lifespan trajectories comprehensively replicate canonical findings and extend them in several directions. Whole-brain EEG confirms one of the most consistently reported effects in the literature, the redistribution of spectral power from slow (δ, θ) [9,30,33,47] to faster dynamics (α, β, γ) [30,33]. Alpha power and PAF follow the expected inverted-U, rising steeply through childhood, peaking in early adulthood, and declining thereafter, two of the strongest known age effects on neurophysiological spectra [31,47]. The theta-alpha trajectories cross near young adulthood, after which theta reverses at the midlife inflection point, a crossover previously linked to later-life cognitive decline [32,34]. Aperiodic components (1/f slope and intercept) offer a band-agnostic view of this shift, replicating the age-related redistribution [29,31] and mirroring narrow-band powers in both trajectory shape and inflection timing, band ratios reproduced the same slow-to-fast reorganization [6,19,35,48]. Sex-specific trajectories were highly similar across all features and regions (0/143 shape differences after FDR correction; small level offsets in 23% of comparisons but feature- and region-specific), with no hemispheric asymmetries detected and only the expected eyes-open vs eyes-closed offsets, focal effects at spatial scales finer than the present regional aggregation cannot be excluded [26].

Beyond trajectory replication and extension, a recurrent theme across clinical cohorts is the inadequacy of group-level spectral contrasts for resolving the heterogeneity of most neuropsychiatric diagnoses [13,16,25]. Normative modelling addresses this not by improving group separation but by transforming the question, rather than asking whether a group differs from controls on average, it asks how far, and in which direction, each individual deviates from their age-, sex-, and context-conditional expectation[12]. This reframing is particularly consequential where diagnostic categories aggregate multiple developmental trajectories and mechanistic pathways, and where the same spectral phenotype may arise through distinct biological routes [49]. A major challenge for generalizable norms is sampling bias, many neuroscience studies recruit highly selected subsets, typically young, educated individuals without chronic conditions [50], anchoring definitions of normality to unrepresentative extremes. We mitigated this by building norms from ten independent datasets, explicitly modelling cross-site

variability, including individuals without formal diagnostic labels, and verifying transferability out of sample [51].This allows us to detect individual-level and group-level differences against a common normative lifespan reference.

Neurocognitive disorders produce the strongest and most consistent deviations

Alzheimer's disease and FTD showed the strongest deviation profiles in both univariate and multivariate analyses, the clearest clinical promise of spectral EEG within a normative framework. The canonical spectral slowing pattern in Alzheimer's disease was unambiguously confirmed, with medium-to-large effect sizes across nearly all features, replicating the established phenotype of neurocognitive decline [3,37,52]. Band ratios amplified these patterns [35]. We extend this literature by providing the first normative-referenced characterization of aperiodic EEG components in Alzheimer's disease [7], the 1/f slope was steeper than expected, reflecting a relative concentration of power at low frequencies that is mechanistically distinct from, though consistent with, narrow-band slowing, and the 1/f intercept showed one of the largest deviations across any feature. These constitute a complementary, band-agnostic marker of the spectral redistribution underlying neurocognitive decline [53], opening a new dimension for tracking progression against age-expected trajectories. A lifespan EEG normative framework offers a practical, first-line tool to quantify functional deviations, support early detection, and monitor progression, situating each individual against their age- and sex-appropriate expectation rather than an undifferentiated group mean. FTD followed the same directional profile with attenuated magnitudes. Critically, PAF showed no deviation in FTD, in direct contrast to Alzheimer's disease, one of the most reliable spectral differentiators between the two, consistent with contemporary literature [52,54] and with the view that FTD involves less posterior cortical dysfunction. We also report the first normative-referenced aperiodic findings in FTD, the 1/f intercept showed a difference the slope of this feature did not, suggesting a partially distinct broadband profile. Overall our finding suggest that both conditions diverge strongly from the population reference but occupy substantially overlapping regions of deviation space [55].

Mental health conditions reveal heterogeneous and overlapping profiles

The null result for the theta/beta ratio in ADHD carries the broadest implications for the field. It is the only spectral EEG measure with FDA clearance as a diagnostic aid for ADHD [40], yet has remained contested as either an absolute biomarker or a subtype stratifier [41]. In our study, the largest normative-referenced test to date, the theta/beta ratio in ADHD did not differ from normative expectation, directly challenging its diagnostic standing. This aligns with meta-analytic evidence of declining theta/beta effect sizes as study quality and sample size increase[41], what had appeared reliable in smaller studies dissolves under a large, covariate-adjusted normative comparisons. Theta power itself remained elevated, confirming the most replicated narrow-band finding in ADHD [6,38,39] while the theta/alpha and fast/slow ratios proved more sensitive to the observed redistribution. More broadly, ADHD showed uniformly small effect sizes with pronounced intraclass variability, suggesting at least two spectral subgroups, one following literature consensus (elevated theta, suppressed delta) and another with subtler or absent abnormalities. ADHD is etiologically too heterogeneous to be treated as a single spectral class[21,56] and only subdivision can reconcile small univariate effects with the neurophysiological variation observed in practice. We also report elevated alpha power, disputing the hypothesis of reduced alpha activity in ADHD [38,39]. Although effect sizes in the alpha literature have been modest and variable [25,38] the scale of the present study warrants serious consideration, pending replication in well-characterized subgroups.

ADHD and ASD showed strikingly similar profiles, suppressed delta, elevated theta, and above-norm alpha, with no feature-level difference reaching significance in direct comparison, and multivariate classifiers yielding only weak separability. ASD additionally showed gamma elevation, confirming a strong finding in the literature [42,44] with the fast/slow ratio as the only significant ratio. This overlap is consistent with shared developmental trajectories and elevated comorbidity [20,22,44] and with the growing recognition that diagnostic boundaries do not map onto discrete spectral phenotypes [2,25,39,42,43]. Tested against the same normative reference, the consistent directionality suggests this resemblance is systematic rather than stochastic. In ASD, the framework introduced aperiodic features into a predominantly narrow-band literature, with results that concorded only piecewise with prior work, expected given the developmental and mechanistic pathways the category aggregates.

Anxiety and PTSD produced the sparsest group-level profiles. For anxiety, only alpha power, the 1/f intercept, and the fast/slow ratio reached significance. The elevated 1/f intercept is, to our knowledge, the first normative-referenced aperiodic characterization across the anxiety spectrum and is consistent with the hyperarousal and attentional hypervigilance characteristic of the condition [57]. Its topographic consistency supports a distributed rather than focal substrate, and speaks to an unresolved question in the literature where both increased and decreased alpha have been reported [23,25,58], modest above-norm alpha combined with aperiodic elevation suggests 1/f dynamics may capture aspects of anxious arousal not reflected in conventional band powers. PTSD produced no features surviving FDR correction, deviation directions broadly matched anxiety (below-norm delta, above-norm theta, elevated 1/f intercept), with PAF showing the largest absolute effect. This null is consistent with the heterogeneity of trauma-related psychopathology [59], the small cohort, and the possibility that the most informative PTSD markers are topographic or asymmetric rather than spectral. Both cohorts were restricted to a narrow age range, so developmental inferences must be treated with caution, a limitation that does not apply to the neurodevelopmental and neurocognitive conditions studied across their full clinical trajectories.

Strengths and Limitations

The principal strength of this work is its scale and scope. Built on 3,973 individuals spanning ages 1-82 across ten acquisition sites, the normative reference is the largest and most age-comprehensive harmonized EEG dataset reported to date. Modelling 231 feature–region combinations with GAMLSS estimates the full conditional distribution rather than only the mean, yielding well-calibrated individual z-scores that transfer robustly to held-out data. The inclusion of aperiodic components alongside narrow-band powers and ratios provides a more thorough account of spectral dynamics than any previous lifespan normative effort, and the ADHD cohort (n = 1,034) is the largest normative-referenced evaluation in any neurodevelopmental condition to date, with power to challenge longstanding claims such as the diagnostic utility of the theta-beta ratio [6,40,41].

Limitations warrant acknowledgement. The neurocognitive cohorts are modest making older-age estimates less stable and replication necessary, particularly for the novel aperiodic findings. The

PTSD and anxiety cohorts were restricted to ages 5-22, precluding lifespan inference. Spatial resolution is limited to eleven lobar regions owing to variable electrode standards across sites [26] (Supplementary Table S1), and eyes-open data were unavailable for neurocognitive groups, preventing recording-condition comparisons where they may be most informative. All datasets were collected in clinical or research contexts; truly population-representative sampling [50], including subclinical individuals, remains an aspiration. Residual muscle artifact in the gamma range cannot be excluded, so the elevated gamma finding in ASD should be interpreted with caution. Finally, this framework captures spectral features only; integration with connectivity, temporal dynamics, event-related responses, structural imaging, and genetics will be necessary to realize the full potential of individualized normative characterization.

Conclusion

We introduce a lifespan normative reference for resting-state spectral EEG that unifies decades of research within a scalable framework and extends it in clinically meaningful directions (Figure 5). Neurocognitive disorders yield large, consistent deviation profiles, with the theta-alpha ratio and newly characterized aperiodic components emerging as the most sensitive markers of neurodegeneration. Neurodevelopmental and mental health conditions, by contrast, produce small, heterogeneous, overlapping profiles that group-level contrasts cannot reliably resolve, and the null theta-beta finding in over one thousand individuals with ADHD directly challenges a widely cited biomarker claim. Together, these results argue for a shift from group-average biomarker discovery toward individual-level normative profiling in EEG for which this framework provides a principled, transferable foundation.

Acknowledgements

This work was supported by the German Research Foundation (DFG) Emmy Noether Programme (513851350, TW), the BMBF/DLR project FEDORA (01EQ2403G, TW), and the Carl Zeiss Foundation (P2022-00-087, TW). Computational resources were provided by the BMBF-funded de.NBI Cloud within the German Network for Bioinformatics Infrastructure (de.NBI; grants

031A532B, 031A533A, 031A533B, 031A534A, 031A535A, 031A537A–D, 031A538A). The authors thank Nitin Sharma and Richard Dinga for insightful discussions on GAMLSS modelling, and Selena Singh for thoughtful comments on a near-final version of the manuscript. A language model was used to assist with editing for clarity and the authors take full responsibility for the content and its accuracy. The authors declare no competing interests.

Author Contributions

F.M. and T.W. conceived the study and designed the overall analytical framework. F.M. implemented the data preprocessing, large-scale modelling, and statistical analyses. T.W. guided the methodological development and supervised the project. F.M. lead and T.W. contributed to data curation and dataset development. F.M. and T.W. jointly interpreted the results and wrote the first manuscript. All authors provided critical feedback on the interpretation of the results, contributed to manuscript revision, and approved the final submission.

Data and Code Availability

All EEG datasets are publicly available through OpenNeuro under the accession identifiers in Supplementary Table S1. Derived data (fitted model parameters, individual z-scores, cleaned analysis files) and analysis code (preprocessing, GAMLSS modelling, post-hoc statistics) will be released at https://github.com/francescomallus/sqEEGNorms and archived at Zenodo upon acceptance. The framework builds on GAMLSS, FOOOF/specparam, MNE-Python, and PyPREP. Source data for all figures are provided with the paper. Code requests prior to acceptance can be addressed to the corresponding authors.

Methods

Estimating norms across the reference samples

We modelled resting-state EEG with eyes-open and eyes-closed from a large (n = 3,973, 63% female) multi-site dataset, with an age range of 1-82 years, spanning 10 different research centers across the globe. The complete dataset comprises 10 subsets, each part of an independent study available either fully open access or limited access through online repositories such as OpenNeuro (https://openneuro.org/, Supplementary Table S1). Each study was thoroughly evaluated for inclusion feasibility and downstream processing inclusion. Diagnostic procedures used by each contributing study, on which our reference-cohort selection relied, as well as the criteria defining the pathological cohorts, are detailed in Supplementary Note S1. Acquisition device and recording location were encoded jointly as a single site factor in the regression models, remaining study-specific differences were addressed in preprocessing. The dataset was split into (i) a reference cohort for training normative models (n = 1,427, 64% female); (ii) a held-out reference cohort without a diagnosis (n = 400, 64% female) and with multiple diagnosed conditions (iii) (n = 2146, 63% female; Figure 1).

To address sampling bias, we selected "control" or "healthy" individuals from each included study and added a small proportion (<20%) of non-diagnosed samples. This latter group was included to deliberately introduce uncertainty into the training data and to push model representativeness toward a broader population. Because these individuals lacked clinical assessment, this subset may include under-represented diagnostic groups that are difficult to categorize, or conditions with symptoms subtle enough to have little or no measurable impact on everyday functioning.

Furthermore, by aggregating data from studies with different original aims, we implicitly incorporate multiple definitions of "healthy" that may complement one another. For example, participants classified as healthy in a study focused on Alzheimer's disease may still have co-occurring conditions such as ADHD or an anxiety subtype. Together, these tolerated "impurities" in the training set help us move beyond the case-control paradigm and the increasingly outdated notion of a single "healthy" population, supporting instead an individualized approach in which deviations are quantified relative to a heterogeneous reference population.

Preprocessing and harmonization

Key to multi-site high dimensional data modelling is preprocessing. We investigated various denoising and harmonization pipelines and decided for a series of preprocessing and feature extraction steps that are commonly chosen in similar workflows [13,16,60], to maximize efficacy while keeping the study simple and reproducible. Raw signals were cleaned using the PREP automatic denoising pipeline [60] for re-referencing and denoising, with RANSAC [61] for automatic bad-channel rejection and subsequent spherical interpolation. Each channel was resampled at 200Hz and then filtered with a notch filter at the local power-line frequency (50 or 60 Hz, depending on site) and a 0.5–50 Hz zero-phase FIR bandpass filter (Hamming window, 53 dB stopband attenuation) to retain the conventional EEG frequency range. Clean EEG recordings were segmented into non-overlapping 8-second epochs, in line with common practice where 2–8 s resting-state segments are used to balance low-frequency resolution, stationarity, and spectral reliability [62]. We additionally ran an independent component analysis (ICA) pipeline to reduce ocular and spurious peak artifacts; results were produced in parallel but showed no substantial differences from the base pipeline. ICA was fit on a 1-Hz high-pass–filtered copy of the EEG (FastICA, maximizing non-Gaussianity). Ocular components were identified using, in order of availability, EOG channels, Fpz, or the mean of Fp1/Fp2; if none were available, no EOG-based exclusion was performed. Identified components were excluded and the solution was applied to the original (non–high-pass) data with identical channel order.

Power spectra and relative narrow-band ratios were calculated via Welch's periodogram method (Hamming 2-second window, 50% overlap, 0.5 Hz resolution). Power spectral density estimates were then averaged over the epochs to reduce variance [62]. This choice, paired with the calculation parameters, reduced variability and increased stability of power spectral density estimates (PSD). Average power spectra were then normalized to the total power and narrow-bands relative powers were extracted as integral of the spectrum within fixed frequency ranges. The frequency bands were delta (δ) [0.5,4] Hz, theta (θ) [4,8] Hz, alpha (α) [8,12] Hz, beta (β) [12,32] Hz and gamma (γ) [32,50] Hz. To include further post-hoc evaluations, we modeled both relative band power as linear, as proportion of total signal power (fractional band power; FBP), and in decibel (dB) scale. Peak alpha

frequency (PAF) was extracted using a derivative-based approach. Within the α band, we identified local maxima as frequencies at which the first derivative of the power spectrum changed sign from positive to negative and the second derivative was negative, indicating a concave downward peak. Power ratios were calculated as ratios between channel-wise narrow bands powers and log-scaled (natural logarithm) to facilitate modelling. Aperiodic component 1/f slope and intercept were estimated using FOOOF fitting algorithm [5,63] and fitted over the absolute power spectra, extracted after signal standardization (z-score) [5]. Fitting on standardized epochs prevented amplitude-dependent biases in the aperiodic estimates from propagating into the normative models.

Finally, we used Koessler atlas 3D channels mapping to the MNI space to aggregate channels from different standards [26]. The atlas maps canonical channels to a set of (x,y,z) coordinates that, in turn, refer to 11 lobes. Regions were Frontal right, median, left; Parietal right, median, left; Temporal right, left; Occipital right, median, left (Figure 2b). All 231 features were normalized at the individual level, and data quality was quantified as the percentage of retained ($epochs_{\%}$) fixed-length epochs after automatic rejection.

Normative modelling with Generalized Additive Models for Location, Scale and Shape

We fitted a total of 231 feature-region models, with sex-specific smooth age effects. Each normative trajectory was modeled as a conditional distribution of the response given age, sex, resting-state condition (eyes-open vs eyes-closed), data quality, and acquisition site. To capture not only central tendency but also dispersion, skewness, and kurtosis, we used distributional regression within the GAMLSS framework [64]. We fitted a four-parameter sinh-arcsinh (SHASH) distribution function [65]. It is continuous on $\mathbb{R}$ and flexibly accommodates non-Gaussian responses commonly observed in quantitative EEG features. For each feature-region pair, we modeled $y \sim SHASH(\mu, \sigma, \nu, \tau)$, with

$$\mu \sim pb(age,\ by = sex) + sex + eyes + epochs_{\%} + time_{tot} + R^2_{1/f} + re(site),$$

$$\sigma \sim pb(age, by = sex) + sex + eyes + epochs_{\%} + time_{tot} + R^2_{1/f},$$

$$\nu \sim pb(age, by = sex) + sex + eyes + epochs_{\%} + time_{tot} + R^2_{1/f},$$

$$\tau \sim 1$$

where $pb(\cdot)$ denotes a penalized B-spline smoother over age, fitted separately by sex, and $re(site)$ is a random effect addend capturing site-level shifts in location. Sex, eyes condition, and the continuous quality metric ($epochs_{\%}$) were included as parametric effects in the location, scale, and skewness submodels. Similarly, to inform the model on total original duration of available data (resting state single run EEG), we added $time_{tot}$. Finally, we added R^2 measure from aperiodic component fitting pipeline ($R^2_{1/f}$). The three previous variables were added as additional quality-control covariates disentangled from the site intercept. This provides additional depth into individual-level signal quality. We constrained the kurtosis to an intercept-only specification to balance flexibility with stability.

Model selection proceeded by fitting a sequence of increasingly complex candidate specifications and choosing the simplest model within $\Delta\text{BIC} \leq 10$ of the minimum BIC, supported by residual diagnostics (including normality/QQ-based checks), Filliben correlation, root mean squared error (RMSE), and variance explained (R^2). All diagnostics were computed on the training cohort. This procedure consistently selected the same balanced specification across feature subtypes (narrow-band power, dB power, band ratios, and aperiodic 1/f measures). If the primary specification failed to converge (1% of feature-region pairs), we refit using reduced spline flexibility (lower effective degrees of freedom). We computed the z-scores as:

$$z = \Phi^{-1}\big(F(y \mid x)\big)$$

where $F(\cdot \mid x)$ is the fitted SHASH cumulative distribution function and Φ^{-1} is the standard normal quantile function. Importantly, model selection (distribution family and predictor specification) was performed exclusively on the training cohort using information criteria and training-derived diagnostics; the held-out reference cohort was not used to choose among candidate specifications.

Post-Hoc statistical analyses

For out-of-sample pathological-to-reference analyses, each participant was projected into the normative space by computing model-derived z-scores for every feature-region pair, i.e., standardized deviations from the conditional distribution predicted by age, sex, resting-state condition (eyes-open/closed), data quality, and site. All model fitting and training-only model selection were performed

exclusively on the training reference cohort. An independent held-out non-diagnosed reference cohort (n = 400; 64% female; age 1–72) was reserved and never used during model fitting or selection. This cohort served (i) for post-hoc out-of-sample evaluation and z-score calibration, and (ii) as the empirical normative reference distribution for all diagnosis-versus-reference statistical contrasts. Sex effects were evaluated by contrasting female and male trajectories on the same age grid, quantifying differences with curve-distance metrics (mean absolute difference, RMSE, absolute area between curves, and maximum absolute deviation) and Pearson's correlation as descriptive similarity index. Statistical significance was assessed using circular-shift permutation testing on the absolute-area statistic (2000 permutations, shift along the age grid). Hemispheric and topographic effects were assessed by comparing left-right homologous trajectories and by pairwise region-region comparisons within hemisphere using the same curve metrics. Statistical significance for trajectory-level comparisons was obtained via circular-shift permutation tests on the absolute-area statistic (2000 permutations, shift along the age grid). Because no significant trajectory-level differences emerged between cortical lobes (Supplementary Figures S9–S10), subsequent group-level statistical contrasts were performed on the per-participant mean z-score across the 11 cortical lobes for each feature, rather than on each feature-region pair separately. For each diagnostic cohort, group-level deviations from the held-out reference were tested feature-by-feature using two-sided Mann–Whitney U tests on these region-averaged z-score distributions, with rank-biserial correlation (r) as the effect-size measure. Pathological-to-pathological contrasts were assessed via the same procedure: pairwise two-sided Mann–Whitney U tests between diagnostic groups, on the distributions of the mean z-scores across the 11 cortical lobes for each feature, with rank-biserial correlation as effect size. Multiple comparisons were controlled using Benjamini-Hochberg false discovery rate correction, applied separately within each analysis family across all feature-level tests and across all trajectory-level permutation comparisons.

Multivariate Deviation and Multivariate Classification with Cross-Validation

To quantify global (multivariate) spectral deviations, we calculated the Mahalanobis distance (D^2) using a pairwise feature-matching approach. For each clinical group, we identified the subset of shared features (z) available between that diagnosis and the reference cohort. The reference distribution's mean vector (μ) and covariance matrix (S) were estimated using these shared features.

$$D^2 = (z - \mu)^T \, S^{-1} \, (z - \mu)$$

Mahalanobis distance offers a holistic distance measure for each diagnostic cohort over the whole feature set. Hence, enabling multivariate deviation score, for spectral EEG analyses of pathological phenotypes. For within-category comparisons, such as ADHD vs ASD, we computed a symmetric Mahalanobis distance, defined as the average of the mean distance of Group A from Group B's distribution and Group B from Group A's distribution. To evaluate the discriminative power of normative spectral EEG z-scores, we implemented linear discriminant analysis (LDA) classifiers with least squares solver and Ledoit-Wolf lemma optimizing shrinkage to stabilize covariance estimation, reducing overfitting. LDA maximizes between-class separation relative to within-class variance across all features simultaneously [66]. Three classifier configurations were evaluated. First, binary classifiers for each diagnostic cohort against the held-out reference. Second, a multiclass one-versus-rest classifier across all seven classes (six diagnostic cohorts plus the held-out reference), reporting per-class, micro-average, and macro-average AUC. Third, binary within-category pairwise classifiers (ADHD vs ASD, Alzheimer's disease vs FTD, anxiety vs PTSD) to assess within-category separability. For multivariate classification, per-subject feature vectors were first obtained by averaging z-scores across the 11 lobar regions, yielding one observation per subject per feature. All classifiers then used 10-fold group-aware cross-validation, with folds defined at the subject level to prevent data leakage from repeated recordings. All z-scores used as classifier inputs were derived from normative models fitted exclusively on the training reference cohort; no test-set data influenced model fitting or feature derivation. Classification significance was assessed via subject-level label-permutation testing (10,000 iterations) with Phipson and Smyth corrected p-values, where labels were shuffled at the subject level while preserving class proportions, and per-class p-values were computed as the fraction of permuted AUCs exceeding the observed AUC [67]. Finally, we performed leave-one-feature-out analysis on each binary classifier, quantifying the importance of each spectral feature measuring its contribution to the classification task, as the change in AUC upon its removal (ΔAUC = AUC_baseline - AUC_without_feature).

631 **References**

632 1. Zhang, H., Zhou, Q.-Q., Chen, H., Hu, X.-Q., Li, W.-G., Bai, Y., Han, J.-X., Wang, Y., Liang, Z.-
633 H., Chen, D., Cong, F.-Y., Yan, J.-Q., & Li, X.-L. (2023). The applied principles of EEG analysis
634 methods in neuroscience and clinical neurology. *Military Medical Research*, *10*(1), 67.
635 https://doi.org/10.1186/s40779-023-00502-7

636 2. Livint Popa, L., Dragos, H., Pantelemon, C., Verisezan Rosu, O., & Strilciuc, S. (2020). The role of
637 quantitative EEG in the diagnosis of neuropsychiatric disorders. *J. Med. Life*, *13*(1), 8–15.

638 3. Micanovic, C., & Pal, S. (2014). The diagnostic utility of EEG in early-onset dementia: A systematic
639 review of the literature with narrative analysis. *Journal of Neural Transmission*, *121*(1), 59–69.
640 https://doi.org/10.1007/s00702-013-1070-5

641 4. Duffy, F. H., Hughes, J. R., Miranda, F., Bernad, P., & Cook, P. (1994). Status of quantitative EEG
642 (QEEG) in clinical practice, 1994. *Clinical EEG (Electroencephalography)*, *25*(4), VI–XXII.
643 https://doi.org/10.1177/155005949402500403

644 5. Donoghue, T., Haller, M., Peterson, E. J., Varma, P., Sebastian, P., Gao, R., Noto, T., Lara, A. H.,
645 Wallis, J. D., Knight, R. T., Shestyuk, A., & Voytek, B. (2020). Parameterizing neural power
646 spectra into periodic and aperiodic components. *Nature Neuroscience*, *23*(12), 1655–1665.
647 https://doi.org/10.1038/s41593-020-00744-x

648 6. Picken, C., Clarke, A. R., Barry, R. J., McCarthy, R., & Selikowitz, M. (2020). The Theta/Beta Ratio
649 as an Index of Cognitive Processing in Adults With the Combined Type of Attention Deficit
650 Hyperactivity Disorder. *Clinical EEG and Neuroscience*, *51*(3), 167–173.
651 https://doi.org/10.1177/1550059419895142

652 7. Kopčanová, M., Tait, L., Donoghue, T., Stothart, G., Smith, L., Flores-Sandoval, A. A., Davila-
653 Perez, P., Buss, S., Shafi, M. M., Pascual-Leone, A., Fried, P. J., & Benwell, C. S. Y. (2024).
654 Resting-state EEG signatures of Alzheimer's disease are driven by periodic but not aperiodic
655 changes. *Neurobiology of Disease*, *190*, 106380. https://doi.org/10.1016/j.nbd.2023.106380

656 8. Valdes-Sosa, P. A., Galan-Garcia, L., Bosch-Bayard, J., Bringas-Vega, M. L., Aubert-Vazquez, E.,
657 Rodriguez-Gil, I., Das, S., Madjar, C., Virues-Alba, T., Mohades, Z., MacIntyre, L. C., Rogers, C.,
658 Brown, S., Valdes-Urrutia, L., Evans, A. C., & Valdes-Sosa, M. J. (2021). The Cuban Human Brain

659 Mapping Project, a young and middle age population-based EEG, MRI, and cognition dataset. *Scientific Data*, *8*(1), 45. https://doi.org/10.1038/s41597-021-00829-7
661 9. Li, M., Wang, Y., Lopez-Naranjo, C., Hu, S., Reyes, R. C. G., Paz-Linares, D., Areces-Gonzalez, A., Hamid, A. I. A., Evans, A. C., Savostyanov, A. N., Calzada-Reyes, A., Villringer, A., Tobon-Quintero, C. A., Garcia-Agustin, D., Yao, D., Dong, L., Aubert-Vazquez, E., Reza, F., Razzaq, F. A., … Valdes-Sosa, P. A. (2022). Harmonized-Multinational qEEG norms (HarMNqEEG). *NeuroImage*, *256*, 119190. https://doi.org/10.1016/j.neuroimage.2022.119190
666 10. Rutherford, S., Fraza, C., Dinga, R., Kia, S. M., Wolfers, T., Zabihi, M., Berthet, P., Worker, A., Verdi, S., & Andrews, D. (2022). Charting brain growth and aging at high spatial precision. *Elife*, *11*, e72904.
669 11. Bethlehem, R. A. I., Seidlitz, J., White, S. R., Vogel, J. W., Anderson, K. M., Adamson, C., Adler, S., Alexopoulos, G. S., Anagnostou, E., Areces-Gonzalez, A., Astle, D. E., Auyeung, B., Ayub, M., Bae, J., Ball, G., Baron-Cohen, S., Beare, R., Bedford, S. A., Benegal, V., … Alexander-Bloch, A. F. (2022). Brain charts for the human lifespan. *Nature*, *604*(7906), 525–533. https://doi.org/10.1038/s41586-022-04554-y
674 12. Marquand, A. F., Rezek, I., Buitelaar, J., & Beckmann, C. F. (2016). Understanding Heterogeneity in Clinical Cohorts Using Normative Models: Beyond Case-Control Studies. *Biological Psychiatry*, *80*(7), 552–561. https://doi.org/https://doi.org/10.1016/j.biopsych.2015.12.023
677 13. Tabbal, J., Ebadi, A., Mheich, A., Kabbara, A., Güntekin, B., Yener, G., Paban, V., Gschwandtner, U., Fuhr, P., Verin, M., Babiloni, C., Allouch, S., & Hassan, M. (2025). Characterizing the heterogeneity of neurodegenerative diseases through EEG normative modeling. *Npj Parkinson's Disease*, *11*(1), 117. https://doi.org/10.1038/s41531-025-00957-6
681 14. De Boer, A. A. A., Bayer, J. M. M., Kia, S. M., Rutherford, S., Zabihi, M., Fraza, C., Barkema, P., Westlye, L. T., Andreassen, O. A., Hinne, M., Beckmann, C. F., & Marquand, A. (2024). Non-Gaussian normative modelling with hierarchical Bayesian regression. *Imaging Neuroscience*, *2*, 1–36. https://doi.org/10.1162/imag_a_00132
685 15. Wolfers, T., Beckmann, C. F., Hoogman, M., Buitelaar, J. K., Franke, B., & Marquand, A. F. (2020). Individual differences v. The average patient: Mapping the heterogeneity in ADHD using

normative models. *Psychological Medicine*, *50*(2), 314–323. https://doi.org/10.1017/S0033291719000084

16. Ebadi, A., Allouch, S., Mheich, A., Tabbal, J., Kabbara, A., Robert, G., Lefebvre, A., Iftimovici, A., Rodríguez-Herreros, B., Chabane, N., & Hassan, M. (2025). Beyond homogeneity: Charting the landscape of heterogeneity in neurodevelopmental and psychiatric electroencephalography. *Translational Psychiatry*, *15*(1), 223. https://doi.org/10.1038/s41398-025-03441-0
17. Wolfers, T., Doan, N. T., Kaufmann, T., Alnæs, D., Moberget, T., Agartz, I., Buitelaar, J. K., Ueland, T., Melle, I., Franke, B., Andreassen, O. A., Beckmann, C. F., Westlye, L. T., & Marquand, A. F. (2018). Mapping the Heterogeneous Phenotype of Schizophrenia and Bipolar Disorder Using Normative Models. *JAMA Psychiatry*, *11*(75), 1146–1155. https://doi.org/10.1001/JAMAPSYCHIATRY.2018.2467
18. Ranasinghe, K. G., Cha, J., Iaccarino, L., Hinkley, L. B., Beagle, A. J., Pham, J., Jagust, W. J., Miller, B. L., Rankin, K. P., Rabinovici, G. D., Vossel, K. A., & Nagarajan, S. S. (2020). Neurophysiological signatures in Alzheimer's disease are distinctly associated with TAU, amyloid-β accumulation, and cognitive decline. *Science Translational Medicine*, *12*(534), eaaz4069. https://doi.org/10.1126/scitranslmed.aaz4069
19. Özbek, Y., Fide, E., & Yener, G. G. (2021). Resting-state EEG alpha/theta power ratio discriminates early-onset Alzheimer's disease from healthy controls. *Clinical Neurophysiology*, *132*(9), 2019–2031. https://doi.org/10.1016/j.clinph.2021.05.012
20. Hours, C., Recasens, C., & Baleyte, J.-M. (2022). ASD and ADHD Comorbidity: What Are We Talking About? *Frontiers in Psychiatry*, *13*, 837424. https://doi.org/10.3389/fpsyt.2022.837424
21. American Psychiatric Association. (2013). *Diagnostic and Statistical Manual of Mental Disorders* (Fifth Edition). American Psychiatric Association. https://doi.org/10.1176/appi.books.9780890425596
22. Shephard, E., Tye, C., Ashwood, K. L., Azadi, B., Asherson, P., Bolton, P. F., & McLoughlin, G. (2018). Resting-State Neurophysiological Activity Patterns in Young People with ASD, ADHD, and ASD + ADHD. *Journal of Autism and Developmental Disorders*, *48*(1), 110–122. https://doi.org/10.1007/s10803-017-3300-4

23. Deng, G., Zhou, Z., Song, K., Ai, H., Zhang, J., Nan, Y., & Xu, P. (2026). Childhood electroencephalographic signatures predict distinct developmental trajectories to adolescent anxiety and depression. *Biological Psychiatry*, S0006322326000995. https://doi.org/10.1016/j.biopsych.2026.03.002

24. Kessler, R. C., Berglund, P. A., Demler, O. V., Jin, R., Merikangas, K. R., & Walters, E. E. (2005). Lifetime prevalence and age-of-onset distributions of DSM-IV disorders in the National Comorbidity Survey Replication. *Archives of General Psychiatry*, *62 6*, 593–602.

25. Newson, J. J., & Thiagarajan, T. C. (2019). EEG Frequency Bands in Psychiatric Disorders: A Review of Resting State Studies. *Frontiers in Human Neuroscience*, *12*, 521. https://doi.org/10.3389/fnhum.2018.00521

26. Koessler, L., Maillard, L., Benhadid, A., Vignal, J. P., Felblinger, J., Vespignani, H., & Braun, M. (2009). Automated cortical projection of EEG sensors: Anatomical correlation via the international 10–10 system. *NeuroImage*, *46*(1), 64–72. https://doi.org/10.1016/j.neuroimage.2009.02.006

27. Stasinopoulos, D. M., & Rigby, R. A. (2008). Generalized Additive Models for Location Scale and Shape (GAMLSS) in R. *Journal of Statistical Software*, *23*, 1–46. https://doi.org/10.18637/jss.v023.i07

28. John, E. R., Ahn, H., Prichep, L., Trepetin, M., Brown, D., & Kaye, H. (1980). Developmental Equations for the Electroencephalogram. *Science*, *210*(4475), 1255–1258. https://doi.org/10.1126/science.7434026

29. Leroy, S., Bublitz, V., Von Dincklage, F., Antonenko, D., & Fleischmann, R. (2025). Normative characterization of age-related periodic and aperiodic activity in resting-state real-world clinical EEG recordings. *Frontiers in Aging Neuroscience*, *17*, 1540040. https://doi.org/10.3389/fnagi.2025.1540040

30. Rempe, M. P., Ott, L. R., Picci, G., Penhale, S. H., Christopher-Hayes, N. J., Lew, B. J., Petro, N. M., Embury, C. M., Schantell, M., Johnson, H. J., Okelberry, H. J., Losh, K. L., Willett, M. P., Losh, R. A., Wang, Y.-P., Calhoun, V. D., Stephen, J. M., Heinrichs-Graham, E., Kurz, M. J., & Wilson, T. W. (2023). Spontaneous cortical dynamics from the first years to the golden years.

Proceedings of the National Academy of Sciences, *120*(4), e2212776120. https://doi.org/10.1073/pnas.2212776120

31. Reyes, R. G., Gonzalez, A. A., Wang, Y., Jin, Y., Yasir, S., Bringas-Vega, M. L., Valdes-Sosa, M., Luo, C., Xu, P., Jirsa, V., Yao, D., Minati, L., & Valdes-Sosa, P. A. (2026). Lifespan Development of EEG Alpha and Aperiodic Component Sources is Shaped by the Connectome and Axonal Delays. *National Science Review*, nwag076. https://doi.org/10.1093/nsr/nwag076
32. Tan, E., Troller-Renfree, S. V., Morales, S., Buzzell, G. A., McSweeney, M., Antúnez, M., & Fox, N. A. (2024). Theta activity and cognitive functioning: Integrating evidence from resting-state and task-related developmental electroencephalography (EEG) research. *Developmental Cognitive Neuroscience*, *67*, 101404. https://doi.org/10.1016/j.dcn.2024.101404
33. Cragg, L., Kovacevic, N., McIntosh, A. R., Poulsen, C., Martinu, K., Leonard, G., & Paus, T. (2011). Maturation of EEG power spectra in early adolescence: A longitudinal study: Maturation of EEG. *Developmental Science*, *14*(5), 935–943. https://doi.org/10.1111/j.1467-7687.2010.01031.x
34. Babiloni, C., Binetti, G., Cassarino, A., Dal Forno, G., Del Percio, C., Ferreri, F., Ferri, R., Frisoni, G., Galderisi, S., Hirata, K., Lanuzza, B., Miniussi, C., Mucci, A., Nobili, F., Rodriguez, G., Luca Romani, G., & Rossini, P. M. (2006). Sources of cortical rhythms in adults during physiological aging: A multicentric EEG study. *Human Brain Mapping*, *27*(2), 162–172. https://doi.org/10.1002/hbm.20175
35. Flores-Sandoval, A. A., Davila-Pérez, P., Buss, S. S., Donohoe, K., O'Connor, M., Shafi, M. M., Pascual-Leone, A., Benwell, C. S. Y., & Fried, P. J. (2023). Spectral power ratio as a measure of EEG changes in mild cognitive impairment due to Alzheimer's disease: A case-control study. *Neurobiology of Aging*, *130*, 50–60. https://doi.org/10.1016/j.neurobiolaging.2023.05.010
36. Cassani, R., Estarellas, M., San-Martin, R., Fraga, F. J., & Falk, T. H. (2018). Systematic Review on Resting-State EEG for Alzheimer's Disease Diagnosis and Progression Assessment. *Disease Markers*, *2018*, 1–26. https://doi.org/10.1155/2018/5174815
37. Lindau, M., Jelic, V., Johansson, S.-E., Andersen, C., Wahlund, L.-O., & Almkvist, O. (2003). Quantitative EEG Abnormalities and Cognitive Dysfunctions in Frontotemporal Dementia and

Alzheimer's Disease. *Dementia and Geriatric Cognitive Disorders*, *15*(2), 106–114. https://doi.org/10.1159/000067973

38. Barry, R. J., Clarke, A. R., & Johnstone, S. J. (2003). A review of electrophysiology in attention-deficit/hyperactivity disorder: I. Qualitative and quantitative electroencephalography. *Clinical Neurophysiology*, *114*(2), 171–183. https://doi.org/10.1016/S1388-2457(02)00362-0
39. Clarke, A. R., Barry, R. J., & Johnstone, S. (2020). Resting state EEG power research in Attention-Deficit/Hyperactivity Disorder: A review update. *Clinical Neurophysiology*, *131*(7), 1463–1479. https://doi.org/10.1016/j.clinph.2020.03.029
40. Gloss, D., Varma, J. K., Pringsheim, T., & Nuwer, M. R. (2016). Practice advisory: The utility of EEG theta/beta power ratio in ADHD diagnosis: Report of the Guideline Development, Dissemination, and Implementation Subcommittee of the American Academy of Neurology. *Neurology*, *87*(22), 2375–2379. https://doi.org/10.1212/WNL.0000000000003265
41. Boxum, M., Voetterl, H., Van Dijk, H., Gordon, E., DeBeus, R., Arnold, L. E., & Arns, M. (2024). Challenging the Diagnostic Value of Theta/Beta Ratio: Insights From an EEG Subtyping Meta-Analytical Approach in ADHD. *Applied Psychophysiology and Biofeedback*. https://doi.org/10.1007/s10484-024-09649-y
42. Neo, W. S., Foti, D., Keehn, B., & Kelleher, B. (2023). Resting-state EEG power differences in autism spectrum disorder: A systematic review and meta-analysis. *Translational Psychiatry*, *13*(1), 389. https://doi.org/10.1038/s41398-023-02681-2
43. Dede, A. J. O., Xiao, W., Vaci, N., Cohen, M. X., & Milne, E. (2025). Exploring EEG resting state differences in autism: Sparse findings from a large cohort. *Molecular Autism*, *16*(1), 13. https://doi.org/10.1186/s13229-025-00647-3
44. Wang, J., Barstein, J., Ethridge, L. E., Mosconi, M. W., Takarae, Y., & Sweeney, J. A. (2013). Resting state EEG abnormalities in autism spectrum disorders. *Journal of Neurodevelopmental Disorders*, *5*(1), 24. https://doi.org/10.1186/1866-1955-5-24
45. Fraza, C., Rutherford, S., Bučková, B. R., Beckmann, C. F., & Marquand, A. F. (2025). The promise of quantifying individual risk for brain disorders through normative modeling, a narrative

review. *Neuroscience & Biobehavioral Reviews*, *176*, 106284. https://doi.org/10.1016/j.neubiorev.2025.106284

46. Musaeus, C. S., Engedal, K., Høgh, P., Jelic, V., Mørup, M., Naik, M., Oeksengaard, A.-R., Snaedal, J., Wahlund, L.-O., Waldemar, G., & Andersen, B. B. (2018). EEG Theta Power Is an Early Marker of Cognitive Decline in Dementia due to Alzheimer's Disease. *Journal of Alzheimer's Disease*, *64*(4), 1359–1371. https://doi.org/10.3233/JAD-180300
47. Han, J., Yang, Z., Ma, M., Liang, L., & Li, X. (2025). Developmental changes in spontaneous electrical activity from early to middle childhood and their relation to short-term working memory ability. *International Journal of Psychophysiology*, *215*, 113238. https://doi.org/10.1016/j.ijpsycho.2025.113238
48. Schmidt, M. T., Kanda, P. A. M., Basile, L. F. H., Da Silva Lopes, H. F., Baratho, R., Demario, J. L. C., Jorge, M. S., Nardi, A. E., Machado, S., Ianof, J. N., Nitrini, R., & Anghinah, R. (2013). Index of Alpha/Theta Ratio of the Electroencephalogram: A New Marker for Alzheimer's Disease. *Frontiers in Aging Neuroscience*, *5*. https://doi.org/10.3389/fnagi.2013.00060
49. Genin, K., Grote, T., & Wolfers, T. (2024). Computational psychiatry and the evolving concept of a mental disorder. *Synthese*, *204*(3), 88. https://doi.org/10.1007/s11229-024-04741-6
50. Enzenbach, C., Wicklein, B., Wirkner, K., & Loeffler, M. (2019). Evaluating selection bias in a population-based cohort study with low baseline participation: The LIFE-Adult-Study. *BMC Medical Research Methodology*, *19*(1), 135. https://doi.org/10.1186/s12874-019-0779-8
51. Rutherford, S., Wolfers, T., Fraza, C., Harrnet, N. G., Beckmann, C. F., Ruhe, H. G., & Marquand, A. F. (2024). *To which reference class do you belong? Measuring racial fairness of reference classes with normative modeling* (arXiv:2407.19114; Issue arXiv:2407.19114). arXiv. http://arxiv.org/abs/2407.19114
52. Benussi, A., Cantoni, V., Palacino, F., Altomare, D., Moretti, D. V., Manganotti, P., & Borroni, B. (2026). EEG network reorganization across Alzheimer's disease, frontotemporal dementia, and dementia with Lewy bodies. *Alzheimer's & Dementia: Diagnosis, Assessment & Disease Monitoring*, *18*(1), e70275. https://doi.org/10.1002/dad2.70275

53. Martínez-Cañada, P., Perez-Valero, E., Minguillon, J., Pelayo, F., López-Gordo, M. A., & Morillas, C. (2023). Combining aperiodic 1/f slopes and brain simulation: An EEG/MEG proxy marker of excitation/inhibition imbalance in Alzheimer's disease. *Alzheimer's & Dementia: Diagnosis, Assessment & Disease Monitoring*, *15*(3), e12477. https://doi.org/10.1002/dad2.12477
54. Caso, F., Cursi, M., Magnani, G., Fanelli, G., Falautano, M., Comi, G., Leocani, L., & Minicucci, F. (2012). Quantitative EEG and LORETA: Valuable tools in discerning FTD from AD? *Neurobiology of Aging*, *33*(10), 2343–2356. https://doi.org/10.1016/j.neurobiolaging.2011.12.011
55. Ghassemkhani, K., Saroka, K. S., & Dotta, B. T. (2025). Evaluating EEG complexity and spectral signatures in Alzheimer's disease and frontotemporal dementia: Evidence for rostrocaudal asymmetry. *Npj Aging*, *11*(1), 50. https://doi.org/10.1038/s41514-025-00243-y
56. Insel, T., Cuthbert, B., Garvey, M., Heinssen, R., Pine, D. S., Quinn, K., Sanislow, C., & Wang, P. (2010). Research Domain Criteria (RDoC): Toward a New Classification Framework for Research on Mental Disorders. *American Journal of Psychiatry*, *167*(7), 748–751. https://doi.org/10.1176/appi.ajp.2010.09091379
57. Chandler, D. A., Roach, A., Ellison, A., Husid Burton, E., & Jelsone-Swain, L. (2022). Symptoms of depression together with trait anxiety increase the ability to predict alpha power change between attention and resting states. *International Journal of Psychophysiology*, *182*, 57–69. https://doi.org/10.1016/j.ijpsycho.2022.09.010
58. Knyazev, G. G., Savostyanov, A. N., & Levin, E. A. (2004). Alpha oscillations as a correlate of trait anxiety. *International Journal of Psychophysiology*, *53*(2), 147–160. https://doi.org/10.1016/j.ijpsycho.2004.03.001
59. Gordon, E., Palmer, D. M., & Cooper, N. (2010). EEG Alpha Asymmetry in Schizophrenia, Depression, PTSD, Panic Disorder, ADHD and Conduct Disorder. *Clinical EEG and Neuroscience*, *41*(4), 178–183. https://doi.org/10.1177/155005941004100404
60. Appelhoff, S., Hurst, A. J., Lawrence, A., Li, A., Mantilla Ramos, Y. J., O'Reilly, C., Xiang, L., Dancker, J., Scheltienne, M., Bialas, O., Alibou, N., Agarwal, A., & Veillette, J. (2025). *PyPREP: A Python implementation of the preprocessing pipeline (PREP) for EEG data.* [Python]. https://github.com/sappelhoff/pyprep (Original work published 2018)

61. Fischler, M. A., & Bolles, R. C. (1981). Random sample consensus: A paradigm for model fitting with applications to image analysis and automated cartography. *Communications of the ACM*, *24*(6), 381–395. https://doi.org/10.1145/358669.358692

62. Levy, W. J. (1987). Effect of epoch length on power spectrum analysis of the EEG. *Anesthesiology*, *66*(4), 489–495. https://doi.org/10.1097/00000542-198704000-00007

63. Gyurkovics, M., Clements, G. M., Low, K. A., Fabiani, M., & Gratton, G. (2021). The impact of 1/f activity and baseline correction on the results and interpretation of time-frequency analyses of EEG/MEG data: A cautionary tale. *NeuroImage*, *237*, 118192. https://doi.org/10.1016/j.neuroimage.2021.118192

64. Stasinopoulos, M. D., Rigby, R. A., & Bastiani, F. D. (2018). GAMLSS: A distributional regression approach. *Statistical Modelling*, *18*(3–4), 248–273. https://doi.org/10.1177/1471082X18759144

65. Jones, M. C., & Pewsey, A. (2009). Sinh-arcsinh distributions. *Biometrika*, *96*(4), 761–780. https://doi.org/10.1093/biomet/asp053

66. Tharwat, A., Gaber, T., Ibrahim, A., & Hassanien, A. E. (2017). Linear discriminant analysis: A detailed tutorial. *AI Communications*, *30*(2), 169–190. https://doi.org/10.3233/AIC-170729

67. Phipson, B., & Smyth, G. K. (2010). Permutation P-values Should Never Be Zero: Calculating Exact P-values When Permutations Are Randomly Drawn. *Statistical Applications in Genetics and Molecular Biology*, *9*(1). https://doi.org/10.2202/1544-6115.1585

872 **Figure Captions**

873 **Figure 1: Normative modelling of electroencephalography (EEG) derived spectral features.** Study
874 design, from data aggregation to feature-wise normative models and individualized scoring. (a) Pipeline
875 stages: (i) multi-site EEG data aggregation, (ii) standardized preprocessing and artifact removal, (iii)
876 spectral feature extraction from resting-state recordings, and (iv) GAMLSS normative model
877 construction yielding individualized deviation scores relative to age- and covariate-adjusted population
878 norms. (b) Training dataset: 1,427 individuals (1,891 recordings, 64% female, ages 1–82) from ten
879 independent resting-state EEG datasets, including eyes-closed (EC) and eyes-open (EO) conditions. (c)
880 Dataset composition: held-out non-diagnosed reference controls (n = 400) for out-of-sample model
881 calibration and as empirical reference for clinical contrasts, alongside six diagnostic cohorts (ADHD,
882 ASD, anxiety disorders, PTSD, Alzheimer's disease, FTD). Sites are identified by institution and EEG
883 acquisition system. Together, this design enables normative deviation scoring that is strictly
884 independent of model training.

885

886 **Figure 2: Lifespan trajectories and distributions across spectral features.** Normative centile
887 trajectories resolve whole-brain spectral maturation from infancy to old age, capturing both central
888 tendency and inter-individual variability. (a) Whole-brain 50th percentile trajectories (% of maximum
889 value), averaged over cortical regions for all modeled features, shown separately by sex (solid = male,
890 dotted = female) with 95% confidence intervals (C.I.). The developmental peak (diamond, ~25-35 years
891 with 95% C.I.) marks the convergence of alpha/PAF maxima and fast-band growth deceleration; the
892 mid-life inflection (triangle, ~50 years) marks accelerated delta descent and PAF directional change.
893 Life stages are annotated along the top axis. (b) Regional centile bands (25–75, 10–90, 2.5–97.5
894 percentiles) for eight features, showing the full distributional spread and trajectory across the lifespan.
895 Female, Left Parietal models shown as example. (c) Cortical lobe parcellation for channel aggregation
896 into eleven symmetric cortical regions, following Koessler et al. Together, these trajectories reveal two
897 hallmarks of spectral maturation: a developmental growth spurt until around age 20 and a mid-life
898 inflection between ages 45 and 60 circa.

899

Figure 3. Heterogeneous deviations across neuropsychiatric conditions. Diagnostic cohorts' group-level deviations from normative spectral expectations, at both the univariate feature level and through multivariate classification. (a) Periodic spectral z-score distributions per diagnostic group versus the held-out reference. Statistical testing was performed on subject-level z-scores obtained by averaging across the 11 lobar regions. Z-scores are well-centered for the reference, confirming out-of-sample calibration. The strongest deviations are observed in Alzheimer's disease and FTD. (b) Aperiodic (1/f) z-score distributions; these features have not previously been evaluated normatively across this range of conditions. In (a) and (b): significance above boxes indicates deviation from reference (*$q<0.05$, *$q<0.01$, **$q<0.001$); markers below indicate within-category pairwise comparisons (none significant). (c) Individual-level scatter with 95% confidence ellipses in theta–beta z-score space (bivariate distance space). Placing this established marker pair into a broader cross-diagnostic perspective; only Alzheimer's disease and FTD separate from the reference. (d) Binary LDA classifier ROC curves and AUC, trained with 10-fold subject-level cross-validation, with significance assessed via 10,000-iteration label-permutation testing. (e) Leave-one-feature-out analysis: ΔAUC quantifies each feature's contribution to classification; positive values indicate the feature aids discrimination. Collectively, these analyses reveal a clear hierarchy: neurocognitive disorders produce large, classifiable deviations driven by broadband spectral reorganization, whereas neurodevelopmental and mental-health conditions show diffuse, near-chance profiles that no single feature, nor the full spectral-feature space, can resolve.

Figure 4. Effects of region, sex, recording condition, and age on normative spectral features. Evaluation of the effects of topographical, biological, and experimental covariates on 11-dimensional deviation profiles. (a) Regional classification performance (AUC) per diagnostic group mapped onto 10–20 electrode positions; no significant lobar differences within any group. (b) Mahalanobis distance (D^2, 11 features) per diagnostic group, split by sex (solid = male, hatched = female). Values above violins show effect size (r) and significance for diagnosis versus reference; values below show within-diagnosis sex comparisons (all non-significant). Alzheimer's disease shows the largest multivariate separation ($r = +0.94$). (c) Same as (b), split by recording condition (solid = eyes closed, dotted = eyes open). Marginal effects in ADHD ($r = +0.06$, $q < 0.05$) and anxiety ($r = +0.16$, $q < 0.01$) are negligible

in magnitude. (d) Deviation profiles by age (2-year bins) and recording condition (solid = eyes closed) across diagnostic categories: neurodevelopmental/mental health conditions (top, bottom) maintain stable, low-magnitude deviations across age; neurocognitive conditions (middle) show persistently elevated deviations. These results confirm that multivariate spectral deviation profiles generalize robustly across covariates and primarily reflect intrinsic physiological variation.

Figure 5. A unified lifespan normative reference for spectral EEG across neurocognitive, neurodevelopmental, and mental health conditions. (a) 50th percentile trajectories (q_{50}) with dispersion (σ) for narrow-band powers (δ, θ, α, β, γ in dB), PAF, aperiodic components (1/f slope, intercept), and band ratios (θ/β, θ/α, fast/slow). Arrows denote dominant lifespan trend: decreasing (↓), increasing (↑), or variable (↕). (b) Per-feature deviation profiles across six diagnostic cohorts: direction, effect size (rank-biserial r), and significance (*q<0.05, **q<0.01, ***q<0.001), benchmarked against literature (✓ confirmed, → extended, ✕ disputed, ★ novel). Colored diamonds indicate above-norm (▲) or below-norm (▼) deviations; gray = non-significant; saturation scales with effect size. Neurocognitive disorders show the strongest signatures, with θ/α yielding the largest effect (Alzheimer's: r = +0.79). Novel aperiodic findings are reported for both Alzheimer's disease and FTD. The θ/β ratio fails to reach significance in ADHD (n = 1,034). Anxiety shows a novel 1/f intercept elevation. PTSD shows no significant deviations. Across all cohorts, the convergence of validated findings with the established literature supports the credibility of the results reported here. Taken together, this framework synthesizes a fragmented literature into a unified normative reference, enabling more principled and homogeneous comparisons across studies, and charting a tractable route towards the integration of neuroscientific findings into clinical decision support systems for cost-effective biomarkers derived from quantitative electroencephalography (EEG) recordings.

Figures

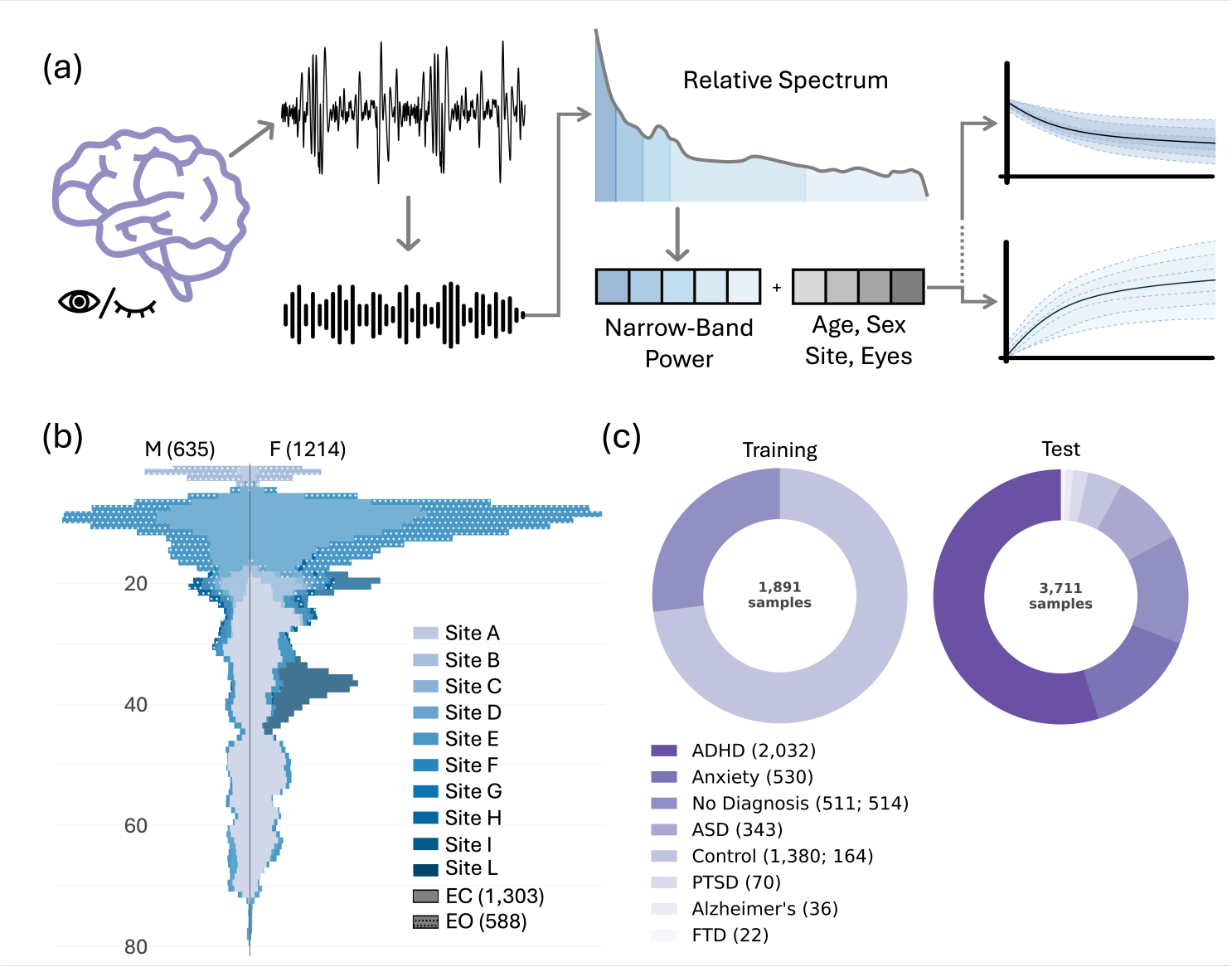


Figure 1

Normative modelling of electroencephalography (EEG) derived spectral features. Study design, from data aggregation to feature-wise normative models and individualized scoring. (a) Pipeline stages: (i) multi-site EEG data aggregation, (ii) standardized preprocessing and artifact removal, (iii) spectral feature extraction from resting-state recordings, and (iv) GAMLSS normative model construction yielding individualized deviation scores relative to age- and covariate-adjusted population norms. (b) Training dataset: 1,427 individuals (1,891 recordings, 64% female, ages 1–82) from ten independent resting-state EEG datasets, including eyes-closed (EC) and eyes-open (EO) conditions. (c) Dataset composition: held-out non-diagnosed reference controls (n = 400) for out-of-sample model calibration and as empirical reference for clinical contrasts, alongside six diagnostic cohorts (ADHD, ASD, anxiety disorders, PTSD, Alzheimer's disease, FTD). Sites are identified by institution and EEG acquisition system. Together, this design enables normative deviation scoring that is strictly independent of model training.

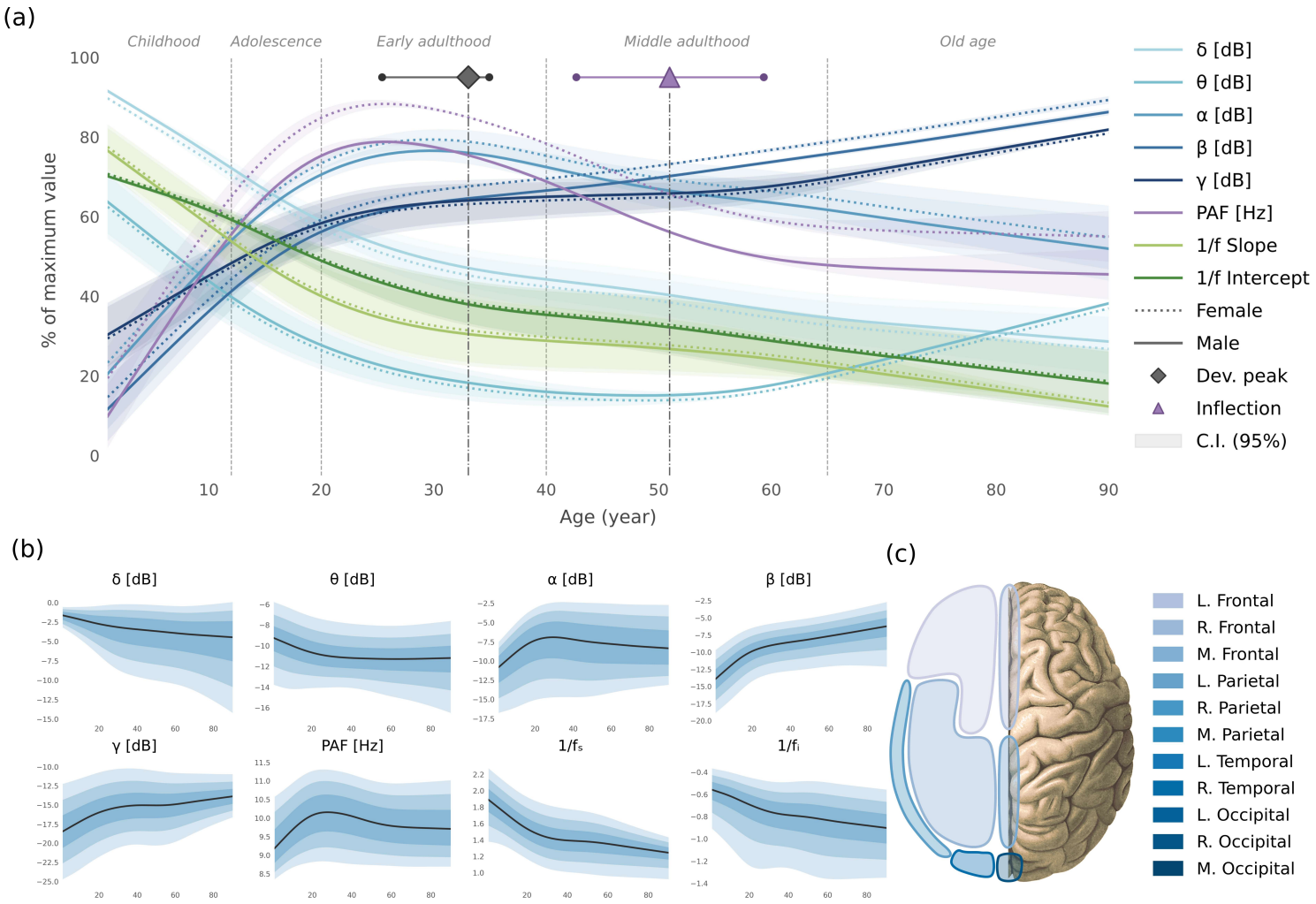


Figure 2

Lifespan trajectories and distributions across spectral features. Normative centile trajectories resolve whole-brain spectral maturation from infancy to old age, capturing both central tendency and inter-individual variability. (a) Whole-brain 50th percentile trajectories (% of maximum value), averaged over cortical regions for all modeled features, shown separately by sex (solid = male, dotted = female) with 95% confidence intervals (C.I.). The developmental peak (diamond, ~25-35 years with 95% C.I.) marks the convergence of alpha/PAF maxima and fast-band growth deceleration; the mid-life inflection (triangle, ~50 years) marks accelerated delta descent and PAF directional change. Life stages are annotated along the top axis. (b) Regional centile bands (25–75, 10–90, 2.5–97.5 percentiles) for eight features, showing the full distributional spread and trajectory across the lifespan. Female, Left Parietal models shown as example. (c) Cortical lobe parcellation for channel aggregation into eleven symmetric cortical regions, following Koessler et al. Together, these trajectories reveal two hallmarks of spectral maturation: a developmental growth spurt until around age 20 and a mid-life inflection between ages 45 and 60 circa.

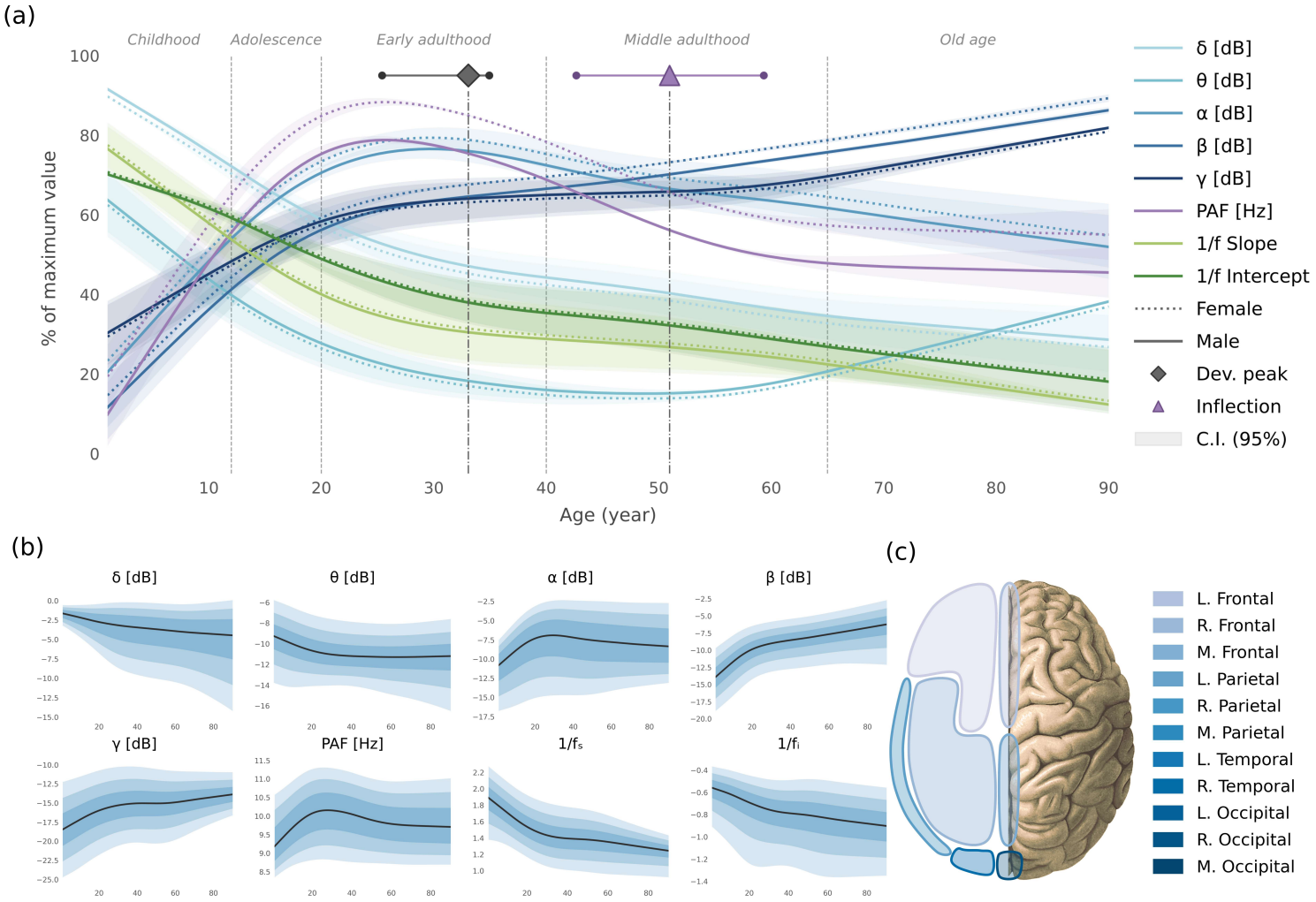

(a)
Childhood
Adolescence
Early adulthood
Middle adulthood
Old age
% of maximum value
Age (year)
δ [dB]
θ [dB]
α [dB]
β [dB]
γ [dB]
PAF [Hz]
1/f Slope
1/f Intercept
Female
Male
Dev. peak
Inflection
C.I. (95%)
(b)
δ [dB]
θ [dB]
α [dB]
β [dB]
γ [dB]
PAF [Hz]
1/fs
1/fi
(c)
L. Frontal
R. Frontal
M. Frontal
L. Parietal
R. Parietal
M. Parietal
L. Temporal
R. Temporal
L. Occipital
R. Occipital
M. Occipital

Figure 2

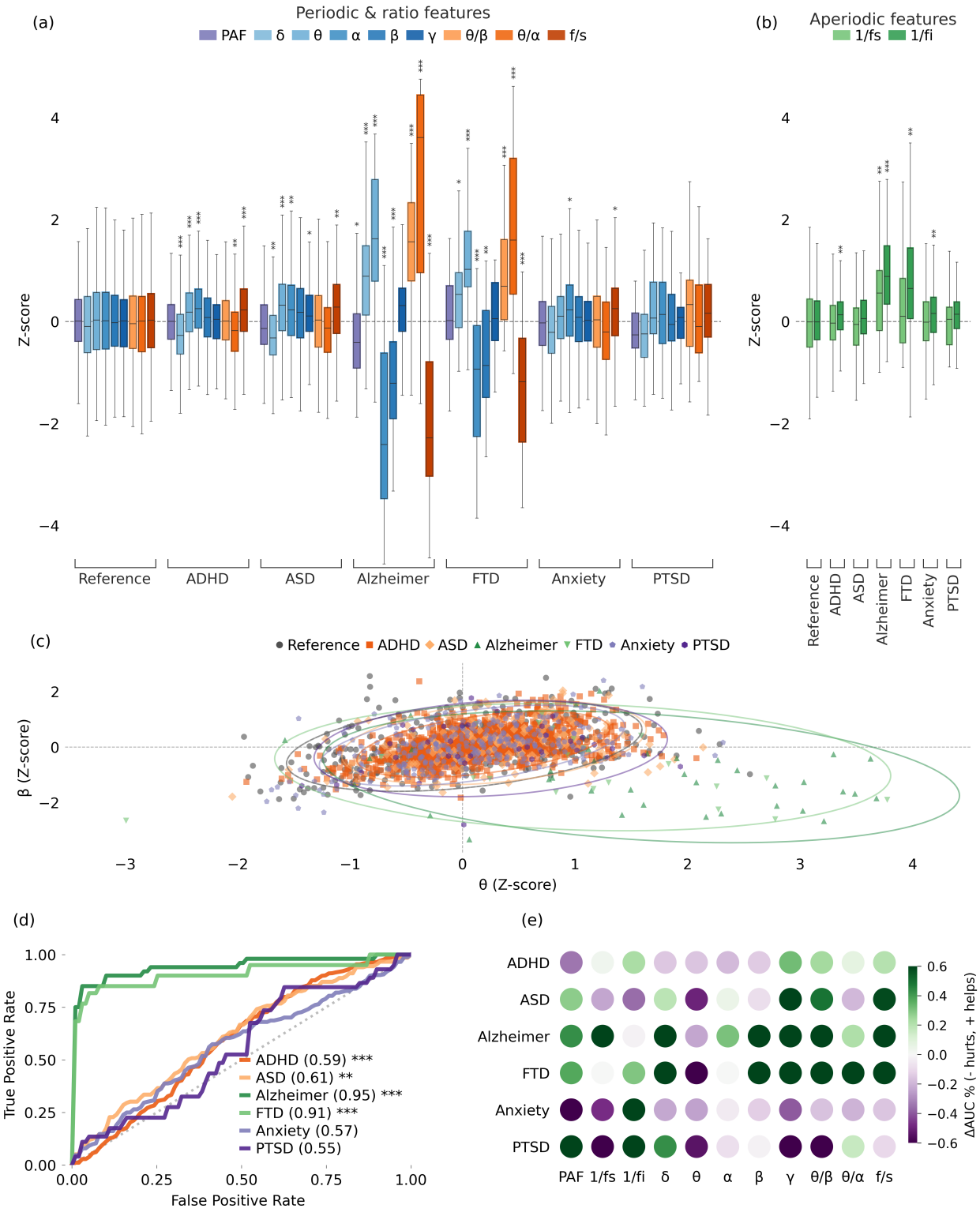


Figure 3

Heterogeneous deviations across neuropsychiatric conditions. Diagnostic cohorts' group-level deviations from normative spectral expectations, at both the univariate feature level and through multivariate classification. (a) Periodic spectral z-score distributions per diagnostic group versus the held-out reference. Statistical testing was performed on subject-level z-scores obtained by averaging across the 11 lobar regions. Z-scores are well-centered for the reference, confirming out-of-sample

calibration. The strongest deviations are observed in Alzheimer's disease and FTD. (b) Aperiodic (1/f) z-score distributions; these features have not previously been evaluated normatively across this range of conditions. In (a) and (b): significance above boxes indicates deviation from reference (*q<0.05, *q<0.01, **q<0.001); markers below indicate within-category pairwise comparisons (none significant). (c) Individual-level scatter with 95% confidence ellipses in theta–beta z-score space (bivariate distance space). Placing this established marker pair into a broader cross-diagnostic perspective; only Alzheimer's disease and FTD separate from the reference. (d) Binary LDA classifier ROC curves and AUC, trained with 10-fold subject-level cross-validation, with significance assessed via 10,000-iteration label-permutation testing. (e) Leave-one-feature-out analysis: ΔAUC quantifies each feature's contribution to classification; positive values indicate the feature aids discrimination. Collectively, these analyses reveal a clear hierarchy: neurocognitive disorders produce large, classifiable deviations driven by broadband spectral reorganization, whereas neurodevelopmental and mental-health conditions show diffuse, near-chance profiles that no single feature, nor the full spectral-feature space, can resolve.

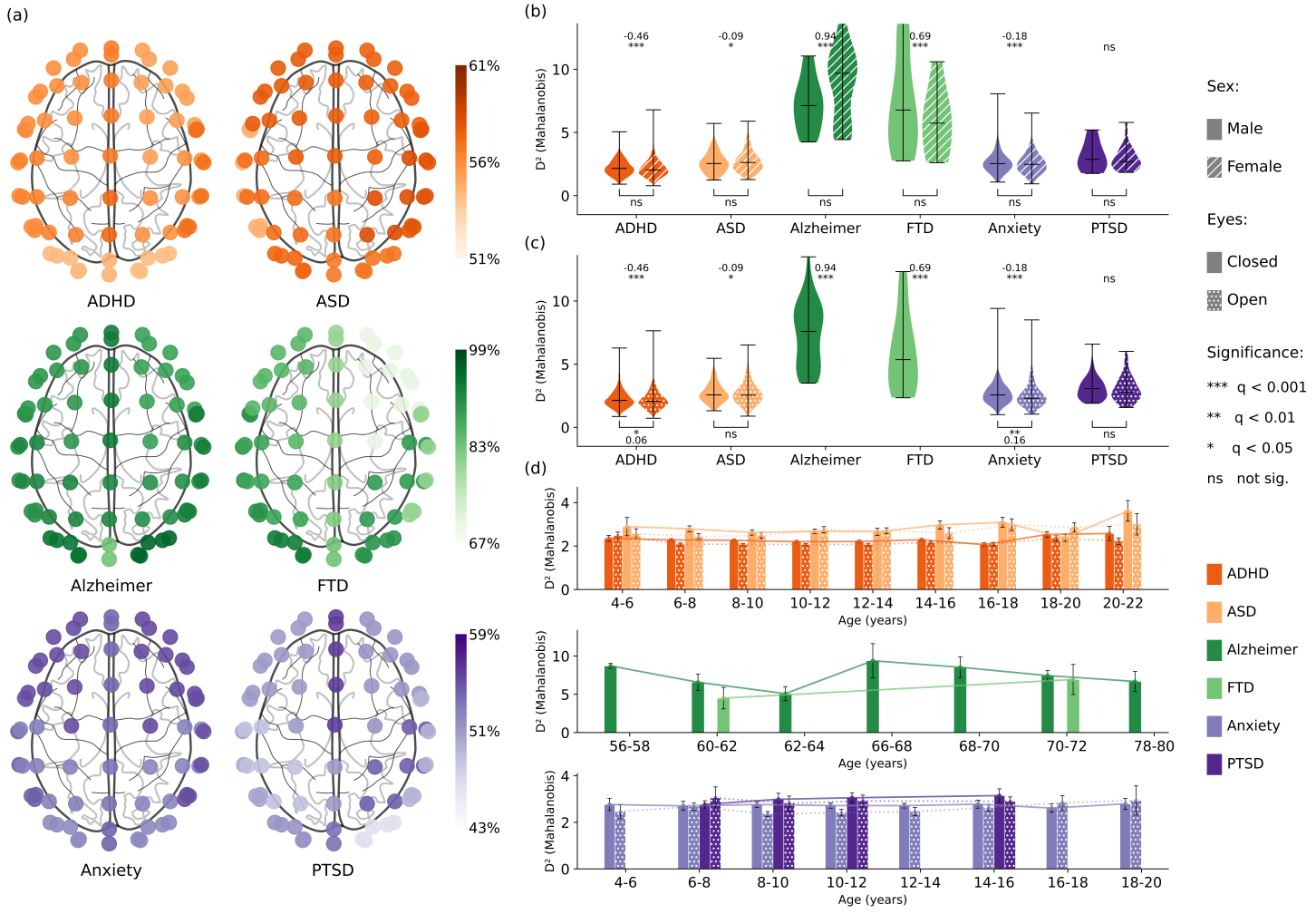


Figure 4

Effects of region, sex, recording condition, and age on normative spectral features. Evaluation of the effects of topographical, biological, and experimental covariates on 11-dimensional deviation profiles.

(a) Regional classification performance (AUC) per diagnostic group mapped onto 10–20 electrode positions; no significant lobar differences within any group. (b) Mahalanobis distance (D^2, 11 features) per diagnostic group, split by sex (solid = male, hatched = female). Values above violins show effect size (r) and significance for diagnosis versus reference; values below show within-diagnosis sex comparisons (all non-significant). Alzheimer's disease shows the largest multivariate separation (r = +0.94). (c) Same as (b), split by recording condition (solid = eyes closed, dotted = eyes open). Marginal effects in ADHD (r = +0.06, q < 0.05) and anxiety (r = +0.16, q < 0.01) are negligible in magnitude. (d) Deviation profiles by age (2-year bins) and recording condition (solid = eyes closed) across diagnostic categories: neurodevelopmental/mental health conditions (top, bottom) maintain stable, low-magnitude deviations across age; neurocognitive conditions (middle) show persistently elevated deviations. These results confirm that multivariate spectral deviation profiles generalize robustly across covariates and primarily reflect intrinsic physiological variation.

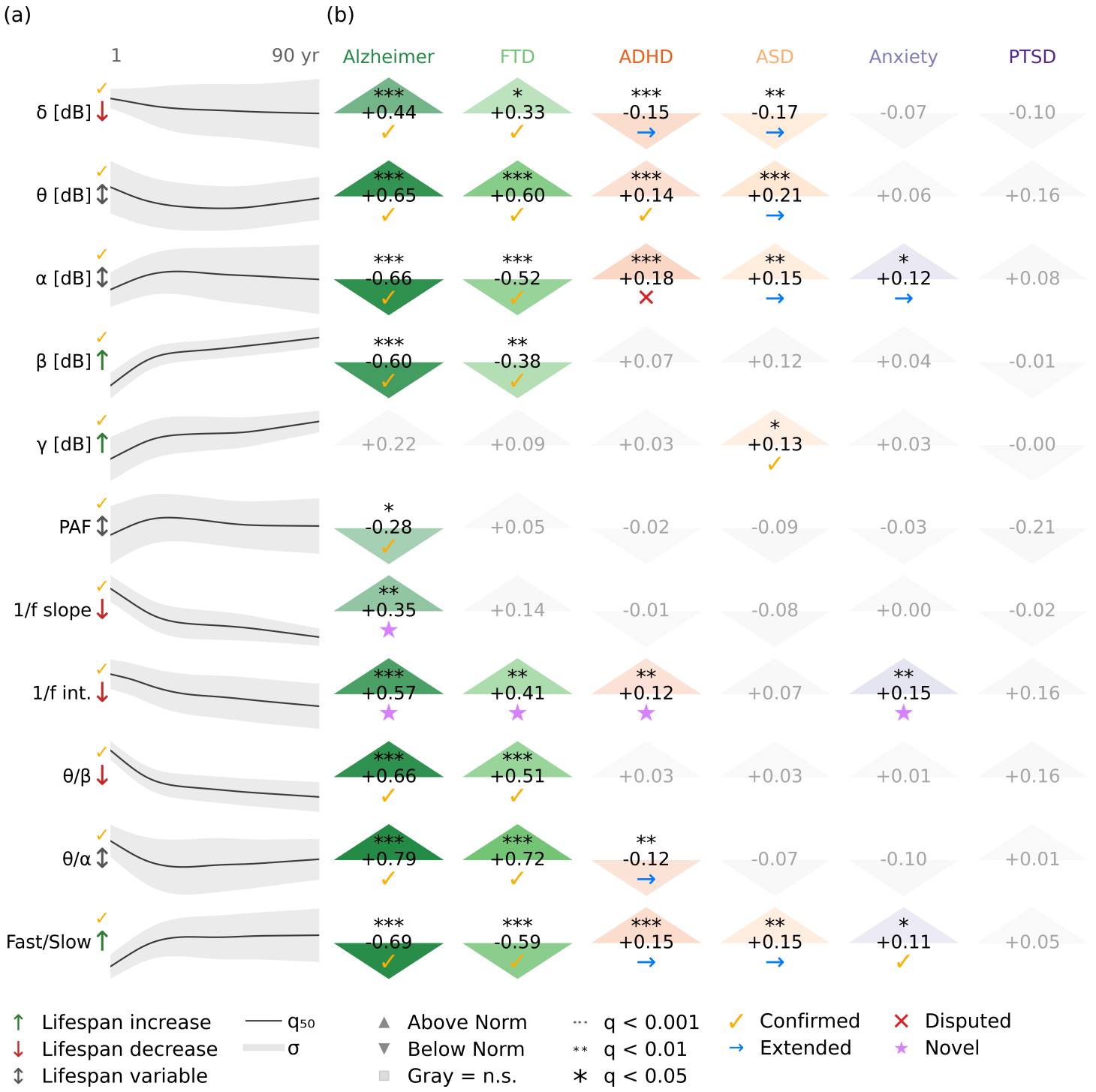


Figure 5

A unified lifespan normative reference for spectral EEG across neurocognitive, neurodevelopmental, and mental health conditions. (a) 50th percentile trajectories (q50) with dispersion (σ) for narrow-band powers (δ, θ, α, J3, γ in dB), PAF, aperiodic components (1/f slope, intercept), and band ratios (θ/J3, θ/α, fast/slow). Arrows denote dominant lifespan trend: decreasing (↓), increasing (↑), or variable (↕). (b) Per-feature deviation profiles across six diagnostic cohorts: direction, effect size (rank-biserial r), and significance (*q<0.05, **q<0.01, ***q<0.001), benchmarked against literature (✓ confirmed, → extended, ✕ disputed, ★ novel). Colored diamonds indicate above-norm (▲) or below-norm (▼) deviations; gray =

non-significant; saturation scales with effect size. Neurocognitive disorders show the strongest signatures, with θ/α yielding the largest effect (Alzheimer's: r = +0.79). Novel aperiodic findings are reported for both Alzheimer's disease and FTD. The θ/J3 ratio fails to reach significance in ADHD (n = 1,034). Anxiety shows a novel 1/f intercept elevation. PTSD shows no significant deviations. Across all cohorts, the convergence of validated findings with the established literature supports the credibility of the results reported here. Taken together, this framework synthesizes a fragmented literature into a unified normative reference, enabling more principled and homogeneous comparisons across studies, and charting a tractable route towards the integration of neuroscientific findings into clinical decision support systems for cost-effective biomarkers derived from quantitative electroencephalography (EEG) recordings.

Supplementary Files

This is a list of supplementary files associated with this preprint. Click to download.

- SupMatSpectralNorms.pdf